Switching Frequency Techniques for Universal Ambient Backscatter Networking

Georgios Vougioukas and Aggelos Bletsas, *Senior Member, IEEE*

***Abstract*— This work offers both analog and digital tag modulation schemes and respective receiver designs, for *ultra*-low power, *high* performance, ambient backscatter communications. All proposed techniques are based on simple, but careful, switching frequency control at the tag, allowing for the easy frequency-domain multiple access. First, a digital modulation scheme is offered, namely pseudo-frequency shift keying, assuming illumination from constant envelope-modulated signals and a fully coherent detector is derived along with closed-form probability of error. A second digital modulation scheme is also offered, based on a frequency-shifted form of binary phase shift keying (S-BPSK), relaxing the constant-envelope requirement for the illuminator and an illumination-agnostic detector is derived. Based on S-BPSK, short packet error correction coding is utilized for ambient backscatter communication, for the first time in the literature. It is shown that the proposed coded scheme under *modulated* ambient signal illumination & wireless channel variation, offers tremendous performance gains, i.e., modulation of the ambient signal is helpful. Finally, a third, purely analog, modulation scheme is analyzed, based on FM *remodulation* principles. A low-cost tag is implemented, demonstrating tag-to-receiver ranges up to 26 meters outdoors, power consumption of 24 μWatts in *continuous* operation, able to be interrogated by *any* conventional frequency modulation (FM) receiver. The proposed techniques cover a large variety of omnipresent wireless industry systems, enabling *universal* ambient backscatter and relevant wireless information and power transfer (WIPT) applications.**

***Index Terms*— Backscatter radio, RFID, bistatic, ambient, WIPT.**

I. Introduction

RECENT advances in backscatter (i.e. reflection-based) communications [3] have enabled low-cost, ultra-low power wireless, possibly sensing, devices [4]. Backscatter communications are employed in modern radio frequency identification (RFID) tags. Apart from the RFID industry, due to its inherent ultra-low power characteristics, backscatter communications technology has been exploited in modern wireless sensor network (WSN) implementations [4]–[8] and is a key enabling technology for implementing WIPT systems. Additionally, for the same reasons, it is a well suited candidate for adoption in the constantly growing field of Internet-of-Things (IoT).

Backscatter radio is based on the reflection that a radio frequency (RF) signal undergoes when impinging at an antenna that is (purposely) ill-terminated. When different loads are chosen to terminate tag's antenna and a method for switching between them is provided, different modulation schemes for the reflected signal can be achieved. This scheme achieves communication without utilizing any form of power consuming active components or other signal conditioning units, such as amplifiers, filters or high frequency oscillators, at the tag's side. Ultra-low power communication can be achieved using just an RF switch that varies the termination load of the tag antenna, given (necessary) illumination. Any backscatter communication system consists of the backscatter tag, a reader and an illuminator. The illuminator is an active RF transmitter, which provides the tag(s) with the necessary RF illumination. The reader and the illuminator may be co-located (monostatic setup, as in RFID) or can be separate units, located at different, possibly distant points (bistatic setup [9]–[11]).

Bistatic setups offer flexibility and improve communication range [10], [11], while more than 1 illuminators in *multistatic* setups significantly increase coverage [12], at the expense of installation costs. In contrast to dedicated, unmodulated illuminating signals, *ambient* backscatter, a special case of bistatic backscatter, exploits for RF illumination ambient *modulated* signals, already present "in the air" [13]. Those signals may come from digital television (DTV) broadcasters, FM radio transmitters or other, non-dedicated sources. In [13] illumination from DTV transmissions was exploited and tag-2-tag communication was demonstrated based on simple envelope detection principles, achieving ranges in the order of 60 cm. In [14] multi-antenna and spread spectrum concepts were implemented in an analog, low power manner. Taking advantage of interference cancellation due to exploiting multi antenna techniques, communication rates up to 1 Mbps (for a tag-2-tag communication range of 2 m) were achieved, exploiting an impinged (at the tag antenna) DTV signal of -10 dBm. In a similar manner, using spread spectrum techniques, a communication range of 6 m was achieved at a rate of 3.3 bps for an impinged DTV signal of -15 dBm. Ambient FM illumination from radio stations was exploited in [15], achieving experimental range of 18 m (for analog audio transmission). The tag was a computer connected to a function generator, which in turn drove the RF switch, while an integrated circuit performing the necessary switching

Manuscript received March 15, 2018; revised July 6, 2018; accepted September 6, 2018. Date of publication September 27, 2018; date of current version January 15, 2019. The research work was supported by the Hellenic Foundation for Research and Innovation (HFRI) and the General Secretariat for Research and Technology (GSRT), under the HFRI PhD Fellowship grant (GA. no. 2263). This paper was presented at [1] and [2].

The authors are with the School of ECE, Technical University of Crete, Kounoupidiana Campus, 73100 Crete, Greece. (e-mail: gevougioukas@isc.tuc.gr; aggelos@telecom.tuc.gr).

Color versions of one or more of the figures in this paper are available online at http://ieeexplore.ieee.org.

Digital Object Identifier 10.1109/JSAC.2018.2872383

was designed and simulated. Digital 2 & 4 audio FSK and analog audio backscatter transmission were demonstrated. Work in [1] independently offered the same FM backscattering methodology while additionally providing a full prototype implementation of a purely analog tag comprised of low cost commercial of-the-shelf (COTS) components and able to be directly interfaced to a passive sensing element. Besides providing an ultra-low power tag, selection diversity was exploited to boost the system's performance. Ambient FM illumination was also considered in [16] to showcase properties of specially designed waveforms (perfect pulses), employed at the tag's side.

Ambient backscatter has been recently studied from a theoretical point of view. In [17], on-off keying (OOK) and differential encoding was employed at the tag. Energy detectors were derived based on invoking the central limit theorem (CLT). In [18] the same scheme was employed at the tag, while the ambient illuminator's complex baseband samples were explicitly considered to follow complex normal distribution; 8-phase shift keying (8-PSK) illumination was also considered. Maximum likelihood and energy based detectors were derived *based on the assumption* of either complex normal or 8-PSK illumination. Variance estimation was used for acquiring the necessary parameters for decision. In a same manner, [19] omitted differential encoding and a small number of training bits was used to aid the variance estimation process. The repeating structure of an OFDM-modulated, illuminating signal was exploited in [20], along with the CLT to derive maximum likelihood (ML) detectors for both single and multi-antenna designs. Tag employed BPSK modulation along with a form of differential encoding. Ambient backscatter, utilizing quadrature PSK (QPSK) and quaternary amplitude shift keying (4-ASK) at the tag, was studied from a information-theoretic point of view in [21]. Assuming availability of a receiver dedicated to recovering ambient carrier's information (e.g., access to the output of a television DTV tuner), it was shown that backscattering operation may offer performance gain to the reception of ambient signal from the legacy receiver. A current overview of the growing ambient backscatter literature can be found in [22].

Most of the practical implementations of ambient backscatter systems listed above, offer short communication ranges and require specially designed receivers for tag interrogation/reception. Detector derivation on some of the theoretical studies is conducted under the umbrella of complex normal assumption. Such practice overlooks the underlying structure of the involved signals which may lead to performance loss.

This work offers both analog & digital hybrid (in the sense of combining benefits from different modulations) backscatter modulation schemes to be exploited in ambient backscatter setups. A common denominator for all proposed techniques is *careful* control of switching frequency with which the tag switches the antenna load between two values (Fig. 1). Such technique allows for easy multiplexing of (possibly receiverless) tags/sensors at the frequency domain [4], [8], [10], [11]. Contrary to prior art, signal structure is either explicitly

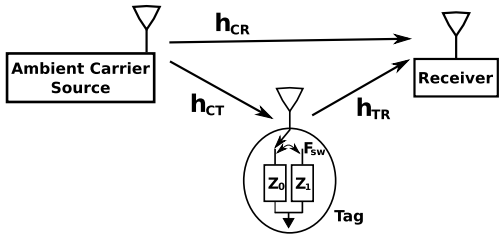

Fig. 1. Carefully controlling the switching frequency at the tag antenna load between two values is the central technique of this work. Ambient modulated illuminator is located away from the receiver. Analog and digital techniques are offered, which accommodate easy multiplexing of multiple tags at the frequency domain.

considered for designing a fully coherent detector, or is completely ignored for deriving an illumination-agnostic, partially coherent detector. Additionally, tag operation is modeled in detail by incorporating all related parameters. Principles from (non-ambient) dedicated illumination, bistatic backscatter communication [8], [11], cannot be directly applied to ambient, *modulated* illumination scenarios, and new detection schemes must be carefully designed, escorting details of tag operation. It has to be emphasized that both [8], [11] considered unmodulated illumination, while the tag utilized FSK modulation. Ambient backscatter is by nature an ultra-low power & cost communication scheme, which enables the realization of WIPT systems [23], [24]. In summary, this work offers:

- A digital, fully coherent, hybrid modulation scheme which will be referred to as pseudo-FSK (P-FSK, Fig. 2-middle), exploiting the multiple access benefits offered by FSK and the limited bandwidth requirements of OOK. Constant envelope structure is assumed for the illuminating signal, which models illuminators utilizing both analog (FM) and digital (FSK, minimum shift keying (MSK), special cases of PSK) modulations. It has to be noted that for an illuminator utilizing a standard BPSK (or QPSK) constellation, the detector will not work.
- A digital, partially coherent, illumination agnostic, hybrid of backscatter FSK and BPSK [12] communication scheme (Fig. 2-right), which will be referred to as shifted BPSK (S-BPSK). Contrary to prior art, the scheme does not require *any* information regarding the ambient carrier or its structure for performing detection. The coherent part of the scheme corresponds to the estimation of a tag & wireless channel-introduced random phase (and an estimation technique is provided). In contrast to the previously mentioned coherent scheme, due to its illumination-agnostic character, S-BPSK can cope with illuminating signals attaining various modulation schemes.
- Exploiting S-BPSK, short packet coding is utilized for the first time (to the best of our knowledge) under an ambient backscatter scenario and detectors are derived. Utilizing the derived detectors under a Bose-Chaudhuri-Hocquenghem (BCH) code, high performance gains are demonstrated, suggesting that the nature of ambient

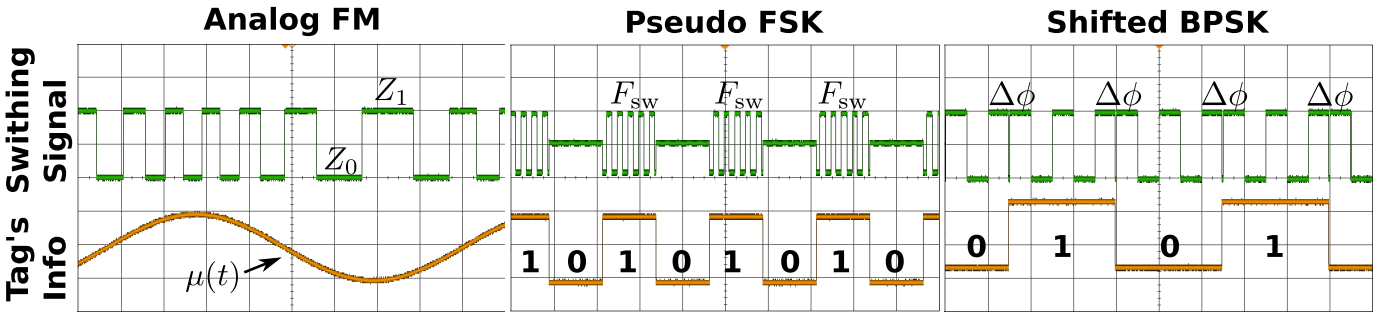

Fig. 2. Suggested switching frequency modulation techniques at the tag for *ultra*-low power, high performance, ambient backscatter communication (FM left, P-FSK middle and S-BPSK right). In the case of P-FSK, the 3rd state between Z_0, Z_1 denotes that any of the two can be chosen for terminating the antenna (for the duration of the bit).

backscatter may be beneficial under certain conditions and improve performance instead of degrading it.

- An analog modulation scheme based on backscatter, (analog) FM (see Fig. 2-left) along with results for the effect of noise and interference at the output of a commodity FM receiver. Results are obtained based on classic FM analysis [25]–[27], while considering however a backscattered signal as input to the FM receiver.
- A full prototype (contrary to laboratory setups presented in prior art) of an ultra-low power tag employing the suggested analog, ambient backscatter scheme, built with low-cost, of-the-shelf components, achieving tag-to-receiver ranges in the order of **26** meters outdoors, able to be interrogated by *any* conventional FM receiver (including FM radio equipped (smart)phones), consuming only $\mathbf{24}\,\mu$Watts in continuous operation.
- The proposed modulation schemes, due to the inherent switching operation, allow for receiver-less tags with easy frequency-based multiple access.
- Contrary to traditional modulation schemes, such as OOK [13], [17], the suggested modulations provide a way for the backscattered signal to be less susceptible to interference from the ambient illuminator signal; due to tag's switching operation, tag signal is backscattered at a different frequency than the ambient illuminator carrier frequency, at the expense of increased power consumption at the tag (compared with conventional OOK). While focusing on communication performance, current off-the-shelf technology [28], [29] allows for ultra-low power, μWatt-consumption implementations of the suggested digital schemes; thus, batteryless operation is enabled, through various energy harvesting methods [30], [31].

Fig. 2 summarizes the tag switching operation for the three studied techniques. It must be noted that the only assumption behind both digital schemes is that the ambient carrier's baseband bandwidth should be much smaller than the switching frequency of the tag (see Eqs. (13), (34)). That is a realistic assumption for a plethora of ambient scenarios, as explained below.

Sec. II offers system model and tag backscatter operation, common to all proposed techniques. P-FSK, S-BPSK and FM remodulation are presented in Secs. III, IV, V, respectively. Performance, examined using both simulations and experimental results, is given in Sec. VI. Finally, work is concluded in Sec. VII.

II. Ambient Backscatter Signal Model

A. Wireless Model

A bistatic backscatter radio setup is considered, as shown in Fig. 1. As it can be seen, the setup is comprised of a carrier source, a tag that is illuminated by the carrier and a reader to recover tag's information from the backscatter signal. Contrary to conventional bistatic setups [10], [11], where the illuminator is a dedicated device emitting an *unmodulated* carrier, this work considers illumination from ambient, *modulated*, RF signals already present "in the air," coming from ambient RF sources (e.g., FM radio stations). This special case of bistatic scatter radio is widely known as ambient backscatter.

Due to relatively small bitrate (in the order of kilobits per second), frequency flat fading channel [32] is assumed, with baseband complex response given by (Fig. 1):

$$h_{\mathrm{p}} = a_{\mathrm{p}}\, \mathsf{e}^{-\mathsf{j}\phi_{\mathrm{p}}}, \quad \mathrm{p} \in \{\mathrm{CR}, \mathrm{CT}, \mathrm{TR}\}, \tag{1}$$

where $a_{\mathrm{CR}}, a_{\mathrm{CT}}, a_{\mathrm{TR}} \in \mathbb{R}_+$ denote the channel fading amplitude parameters and $\phi_{\mathrm{CR}}, \phi_{\mathrm{CT}}, \phi_{\mathrm{TR}} \in [0, 2\pi)$ the respective phases of the corresponding links (where CR denotes the Carrier-to-Reader link, CT the Carrier-to-Tag link and TR the Tag-to-Reader link). Due to the bistatic setup, channel parameters are independent of each other and change every T_{coh} seconds.

The ambient carrier emitter (CE) emits a modulated carrier at frequency F_c, with complex baseband representation given by:

$$\mathsf{c}\,(t) = \mathsf{m}\,(t)\ \mathsf{e}^{-\mathsf{j}(2\pi\Delta F_c t + \Delta\phi_c)}, \tag{2}$$

where $\mathsf{m}\,(t) = m_{\mathrm{ac}}\,(t)\,\mathsf{e}^{\mathsf{j}\Phi_{\mathrm{ac}}(t)}$ is the ambient CE's complex baseband equivalent and ΔF_c, $\Delta\phi_c$ model the carrier frequency and phase offset, respectively, between the ambient CE and the software defined radio (SDR) (reader). The signal impinging on the tag's antenna can be then given by:

$$\mathsf{c}_{\mathrm{tag}}\,(t) = \mathsf{c}\,(t)\ h_{\mathrm{CT}} = a_{\mathrm{CT}}\,\mathsf{e}^{-\mathsf{j}\phi_{\mathrm{CT}}}\ \mathsf{m}\,(t)\ \mathsf{e}^{-\mathsf{j}(2\pi\Delta F_c t + \Delta\phi_c)}. \tag{3}$$

Thus, the received signal at the reader can be expressed as follows:

$$\mathsf{y}_i(t) = \mathsf{c}(t)\, h_{\rm CR} + \mathrm{s}\, \mathsf{c}_{\rm tag}(t)\, \mathsf{x}^i_{\rm tag}(t)\, h_{\rm TR} + w(t), \quad (4)$$

where $\mathsf{x}^i_{\rm tag}(t)$ is the tag's signal, as will be described below, s is the tag's scattering efficiency and $w(t)$ models the thermal noise affecting the received signal. Binary signaling is assumed at the tag and each state is represented by $i \in \{0,1\}$. It should be noted that wireless channel introduced delays are neglected in Eq. (4). That is because either they can be modeled via including them in the random phase introduced by the tag (discussed in the next section) or do not affect subsequent derivation steps.

B. Tag Operation

Consider the case of an RF wave produced by a source with impedance $Z_{\rm source}$. The source is connected to a load, $Z_{\rm load}$. If the load is not matched with the source, i.e $Z_{\rm source} \neq Z^*_{\rm load}$, a portion of the power destined for the load will be reflected back to the source. The amount of reflection depends on the *reflection coefficient*, defined as:

$$\Gamma = \frac{Z_{\rm load} - Z^*_{\rm source}}{Z_{\rm load} + Z_{\rm source}}, \quad (5)$$

The above fact can be exploited to achieve communication. If the RF source is an antenna and a load is chosen in order to end up with reflection of the incident wave, the antenna is forced to reflect. On the other hand, if the load is matched to the antenna, ideally, the load absorbs all the power and no reflection occurs. By carefully choosing the loads and the alternation among them, we can manipulate the reflected signal to end up having certain characteristics.

A tag comprised of an antenna terminated, alternatively, at two different loads Z_0, Z_1 (resulting to Γ_0, Γ_1, respectively), using an RF switch is considered. The switch is driven by a square wave, $q(t)$, with frequency $F^{(i)}_{sw}$ and 50% duty cycle. In that case, it can be shown[1] that tag's signal $\mathsf{x}^i_{\rm tag}(t)$ can be expressed as follows [10], [11]:

$$\mathsf{x}^i_{\rm tag}(t) = m_{\rm dc}\, \mathsf{e}^{\mathsf{j}\theta_{\rm dc}} + m_{\rm tag}\, \mathsf{e}^{\mathsf{j}\theta_{\rm tag}}\, \mathsf{cos}\left(2\pi F^{(i)}_{sw}\, t + \Phi_{\rm t} + \phi_i(t)\right), \quad (6)$$

where $i \in \{0,1\}$. Variable $\Phi_{\rm t}$ models the random phase introduced by tag's operation while $\phi_i(t)$ is purposely introduced to model information that is potentially encapsulated into tag's phase. It must be noted that throughout this work, $\Phi_{\rm t}$ is considered random with $\Phi_{\rm t} \sim \mathcal{U}[0, 2\pi)$, but constant for the duration of a backscattered packet. Parameters $m_{\rm dc}$, $\theta_{\rm dc}$ and $m_{\rm tag}$, $\theta_{\rm tag}$ are given by:

$$m_{\rm dc} = |A_{\rm s} - \frac{\Gamma_0 + \Gamma_1}{2}|, \quad \theta_{\rm dc} = \underline{\angle A_{\rm s} - \frac{\Gamma_0 + \Gamma_1}{2}},$$
$$m_{\rm tag} = \frac{2|\Gamma_0 - \Gamma_1|}{\pi}, \quad \theta_{\rm tag} = \underline{\angle \Gamma_0 - \Gamma_1}, \quad (7)$$

where Γ_0, Γ_1 are the reflection coefficients associated with Z_0, Z_1, respectively and $A_{\rm s}$ is a complex, load-independent parameter that depends on the tag antenna.

[1]By only keeping the fundamental frequency component of $q(t)$, which holds 80% of its power.

III. Coherent P-FSK

In this section a digital, backscatter communication scheme will be studied exploiting as illuminating carrier any modulated, constant envelope signal and the resulting, due to backscatter, modulation will be assumed to be P-FSK, as it will be discussed below.

A. Modulation & Signal Model

In the proposed P-FSK scheme, to backscatter bit "1," tag (similarly to conventional FSK) continuously alternates between the two loads (Z_0, Z_1) at a rate $F_{\rm sw}$, for the duration of the bit $(T_{\rm bit})$. To transmit bit "0," tag simply "rests" its antenna at one of the loads for the same amount of time $(T_{\rm bit})$. Tag modulation is not pure FSK, since during bit "0," the tag simply terminates its antenna at one load state; in that way, bandwidth is reserved. Eq. (6) can represent the above scheme by setting $F^{(1)}_{sw} = F_{\rm sw}$ and $F^{(0)}_{sw} = 0$. Thus, the tag's switching signal for bit $i \in \{0,1\}$ takes the form:

$$\mathsf{x}^{{\rm PF},i}_{\rm tag}(t) = \begin{cases} m_0\, \mathsf{e}^{\mathsf{j}\theta_0}, & i = 0 \\ m_{\rm dc}\, \mathsf{e}^{\mathsf{j}\theta_{\rm dc}} + m_{\rm tag}\, \mathsf{e}^{\mathsf{j}\theta_{\rm tag}}\, \mathsf{cos}\,(2\pi F_{\rm sw} t + \Phi_{\rm t}), & i = 1. \end{cases} \quad (8)$$

No information is carried on the phase of the tag's switching signal so $\phi_i(t) = 0$. It is assumed that for bit "0" the antenna is connected to load Z_0 and parameters m_0, θ_0 are related to that load, tag's antenna and phase $\Phi_{\rm t}$.

A constant envelope-modulated ambient signal is assumed to illuminate the tag(s). Thus, the complex envelope model $\mathsf{m}(t)$ in Eq. (2) takes the following form:

$$\mathsf{m}_{\rm ce}(t) = A_{\rm c} \mathsf{e}^{\mathsf{j}\phi(t)}. \quad (9)$$

Based on Eq. (4), for the duration of a single bit and assuming perfect carrier frequency offset (CFO) correction, the received signal at the reader can be expressed as follows:

$$\mathsf{y}^{\rm PF}_1(t) = \mathsf{e}^{\mathsf{j}\phi(t)} \left[a_{\rm dir} \mathsf{e}^{\mathsf{j}\theta_{\rm dir}} + \hat{m}_{\rm tag} \mathsf{e}^{-\mathsf{j}\hat{\theta}_{\rm tag}} \mathsf{cos}\,(2\pi F_{\rm sw} t + \Phi_{\rm t})\right] + n(t),$$
$$\mathsf{y}^{\rm PF}_0(t) = \mathsf{e}^{\mathsf{j}\phi(t)} \left[\frac{1}{2} a_{\rm CR} A_{\rm c} \mathsf{e}^{-\mathsf{j}(\phi_{\rm CR} + \Delta\phi_c)} + \hat{m}_0 \mathsf{e}^{-\mathsf{j}\hat{\theta}_0}\right] + n(t). \quad (10)$$

Parameters utilized in Eq. (10) are given below:

$$\begin{aligned} \hat{m}_0 &= \frac{1}{2} A_{\rm c}\, \mathrm{s}\, a_{\rm CT}\, a_{\rm TR}\, m_0, \\ \hat{\theta}_0 &= \phi_{\rm CT} + \phi_{\rm TR} - \theta_0 + \Delta\phi_c, \\ a_{\rm dir} \mathsf{e}^{\mathsf{j}\theta_{\rm dir}} &= \frac{1}{2} a_{\rm CR} A_{\rm c} \mathsf{e}^{-\mathsf{j}(\phi_{\rm CR} + \Delta\phi_c)} + \hat{m}_{\rm dc} \mathsf{e}^{-\mathsf{j}\hat{\theta}_{\rm dc}}, \\ \hat{m}_{\rm dc} &= \frac{1}{2} A_{\rm c}\, \mathrm{s}\, a_{\rm CT}\, a_{\rm TR}\, m_{\rm dc}, \\ \hat{\theta}_{\rm dc} &= \phi_{\rm CT} + \phi_{\rm TR} + \Delta\phi_c - \theta_{\rm dc}, \\ \hat{m}_{\rm tag} &= \frac{1}{2} A_{\rm c}\, \mathrm{s}\, a_{\rm CT}\, a_{\rm TR} m_{\rm tag}, \\ \hat{\theta}_{\rm tag} &= \phi_{\rm CT} + \phi_{\rm TR} + \Delta\phi_c - \theta_{\rm tag}. \end{aligned} \quad (11)$$

Term $A_{\rm c}$ is scaled by a factor of $\frac{1}{2}$ due to the homodyne processing and downconversion at the reader [10]. Noise $n(t)$

is a circularly symmetric, additive Gaussian process with power spectral density given by:

$$\mathrm{s_n}\left(F\right)=\begin{cases}\dfrac{N_0}{2}, & |F|\leq W_{\mathrm{rx}}\\ 0, & \text{otherwise,}\end{cases} \tag{12}$$

where W_{rx} denotes the SDR operating bandwidth.

It is also assumed that the complex envelope of the ambient, constant envelope-modulated signal "varies" much slower compared to a complex exponential with frequency F_{sw}. Mathematically,

$$\mathrm{BW}\left(\mathrm{e}^{\mathrm{j}\phi(t)}\right)\ll F_{\mathrm{sw}}, \tag{13}$$

where $\mathrm{BW}\left(\mathrm{e}^{\mathrm{j}\phi(t)}\right)$ denotes the largest frequency component of $\mathrm{e}^{\mathrm{j}\phi(t)}$. For example, in the context of illumination from FM radio stations, where each FM station signal's bandwidth is approximately 100 kHz, switching frequency should be in the order of 1 MHz. Even with existing, off-the-shelf technology, such switching rates may be achieved with small power consumption in the order of 20 μWatt [28], [29].

B. Correlators

Complex baseband samples from the SDR are taken at a sampling rate $F_{\mathrm{s}}=1/T_{\mathrm{s}}$. These samples are expressed as $\mathrm{y}_i^{\mathrm{PF}}[k]=\mathrm{y}_i^{\mathrm{PF}}(kT_{\mathrm{s}})$, $i\in\{0,1\}$. By assumption, noise samples $n[k]$ are distributed as $n[k]\sim\mathcal{CN}\left(0,\sigma_n^2\right)$ with $\sigma_n^2=N_0\,W_{\mathrm{rx}}$ and ambient signal samples are denoted as $\phi(kT_{\mathrm{s}})=\phi[k]$. Two correlators offer sufficient statistics:

$$\begin{aligned}r^+&=\sum_{k=0}^{L-1}\mathrm{y}_i^{\mathrm{PF}}[k]\left(\mathrm{e}^{\mathrm{j}2\pi F_{\mathrm{sw}}kT_{\mathrm{s}}}\right)^*=\sum_{k=0}^{L-1}\mathrm{y}_i^{\mathrm{PF}}[k]\,\mathrm{e}^{-\mathrm{j}2\pi F_{\mathrm{sw}}kT_{\mathrm{s}}},\\ r^-&=\sum_{k=0}^{L-1}\mathrm{y}_i^{\mathrm{PF}}[k]\,\mathrm{e}^{\mathrm{j}2\pi F_{\mathrm{sw}}kT_{\mathrm{s}}},\end{aligned} \tag{14}$$

where $L=\frac{T_{\mathrm{bit}}}{T_{\mathrm{s}}}$ is the bit duration, measured in number of samples.

1) Hypothesis H_0: Under hypothesis H_0 (i.e., bit $i=0$ is backscattered), r^+ can be expanded as:

$$\begin{aligned}r^+=&\left(\frac{1}{2}a_{\mathrm{CR}}A_{\mathrm{c}}\mathrm{e}^{-\mathrm{j}(\phi_{\mathrm{CR}}+\Delta\phi_c)}+\hat{m}_0\mathrm{e}^{-\mathrm{j}\hat{\theta}_0}\right)\\ &\times\underbrace{\sum_{k=0}^{L-1}\mathrm{e}^{\mathrm{j}\phi[k]}\mathrm{e}^{-\mathrm{j}2\pi F_{\mathrm{sw}}kT_{\mathrm{s}}}}_{\overset{(*)}{\approx}0}+\underbrace{\sum_{k=0}^{L-1}n\,[k]\,\mathrm{e}^{-\mathrm{j}2\pi F_{\mathrm{sw}}kT_{\mathrm{s}}}}_{n^+\sim\mathcal{CN}(0,L\sigma_n^2)}=n^+.\end{aligned} \tag{15}$$

Using the assumption of Eq. (13), a relatively "slow" $\mathrm{e}^{\mathrm{j}\phi[k]}$ modulates a "fast" exponential (i.e., F_{sw} is greater than the frequency span of $\mathrm{e}^{\mathrm{j}\phi[k]}$) and thus, the integral of their product tends to zero [26, Ch. 3.2]. In the same way, it can be shown that under H_0, $r^-=n^-$, with $n^-\sim\mathcal{CN}\left(0,L\sigma_n^2\right)$.

2) Hypothesis H_1: Under hypothesis H_1, r^+ is given by:

$$\begin{aligned}r^+=&\,a_{\mathrm{dir}}\mathrm{e}^{\mathrm{j}\theta_{\mathrm{dir}}}\underbrace{\sum_{k=0}^{L-1}\mathrm{e}^{\mathrm{j}\phi[k]}\mathrm{e}^{-\mathrm{j}2\pi F_{\mathrm{sw}}kT_{\mathrm{s}}}}_{\approx0}\\ &+\frac{\hat{m}_{\mathrm{tag}}}{2}\mathrm{e}^{-\mathrm{j}\hat{\theta}_{\mathrm{tag}}}\mathrm{e}^{\mathrm{j}\Phi_{\mathrm{t}}}\sum_{k=0}^{L-1}\mathrm{e}^{\mathrm{j}\phi[k]}\mathrm{e}^{\mathrm{j}2\pi F_{\mathrm{sw}}kT_{\mathrm{s}}}\mathrm{e}^{-\mathrm{j}2\pi F_{\mathrm{sw}}kT_{\mathrm{s}}}\\ &+\frac{\hat{m}_{\mathrm{tag}}}{2}\mathrm{e}^{-\mathrm{j}\hat{\theta}_{\mathrm{tag}}}\mathrm{e}^{-\mathrm{j}\Phi_{\mathrm{t}}}\underbrace{\sum_{k=0}^{L-1}\mathrm{e}^{\mathrm{j}\phi[k]}\mathrm{e}^{-\mathrm{j}2\pi 2F_{\mathrm{sw}}kT_{\mathrm{s}}}}_{\approx0}+n^+\\ =&\,\frac{\hat{m}_{\mathrm{tag}}}{2}\mathrm{e}^{-\mathrm{j}\hat{\theta}_{\mathrm{tag}}}\mathrm{e}^{\mathrm{j}\Phi_{\mathrm{t}}}\sum_{k=0}^{L-1}\mathrm{e}^{\mathrm{j}\phi[k]}+n^+,\end{aligned} \tag{16}$$

due to Eq. (13) and use of $\cos(x)=\frac{1}{2}\left(\mathrm{e}^{\mathrm{j}x}+\mathrm{e}^{-\mathrm{j}x}\right)$. Output r^- of second correlator can be calculated in a similar manner.

C. Statistics

The correlator outputs are summarized below:

$$\begin{aligned}r^+|\mathrm{H}_1&=\frac{\hat{m}_{\mathrm{tag}}}{2}\mathrm{e}^{-\mathrm{j}\hat{\theta}_{\mathrm{tag}}}\mathrm{e}^{\mathrm{j}\Phi_{\mathrm{t}}}\sum_{k=0}^{L-1}\mathrm{e}^{\mathrm{j}\phi[k]}+n^+,\qquad r^+|\mathrm{H}_0=n^+\\ r^-|\mathrm{H}_1&=\frac{\hat{m}_{\mathrm{tag}}}{2}\mathrm{e}^{-\mathrm{j}\hat{\theta}_{\mathrm{tag}}}\mathrm{e}^{-\mathrm{j}\Phi_{\mathrm{t}}}\sum_{k=0}^{L-1}\mathrm{e}^{\mathrm{j}\phi[k]}+n^-,\quad r^-|\mathrm{H}_0=n^-.\end{aligned}$$

To perform coherent detection, parameters $\hat{m}_{\mathrm{tag}}$, $\hat{\theta}_{\mathrm{tag}}$, Φ_{t} as well as $\sum_{k=0}^{L-1}\mathrm{e}^{\mathrm{j}\phi[k]}$ need to be known to the receiver. It can be assumed that due to low chosen bitrate of $R=1/T_{\mathrm{bit}}$ and for a limited number of bits N_{pack}, the variations of the compound channel $\frac{\hat{m}_{\mathrm{tag}}}{2}\mathrm{e}^{-\mathrm{j}\hat{\theta}_{\mathrm{tag}}}\mathrm{e}^{\mathrm{j}\Phi_{\mathrm{t}}}$ may be considered negligible.[2] Assuming that the phase samples are independent and identically distributed (IID) and exploiting the law of large numbers (i.e., large L),

$$\mathbb{E}\left[\mathrm{e}^{\mathrm{j}\phi}\right]\approx\frac{1}{L}\sum_{k=0}^{L-1}\mathrm{e}^{\mathrm{j}\phi[k]}\Leftrightarrow\sum_{k=0}^{L-1}\mathrm{e}^{\mathrm{j}\phi[k]}\approx L\,\mathbb{E}\left[\mathrm{e}^{\mathrm{j}\phi}\right]\triangleq\lambda_{\mathrm{ac}}. \tag{17}$$

In view of Eq. (17), term $\sum_{k=0}^{L-1}\mathrm{e}^{\mathrm{j}\phi[k]}$ can be also considered constant during multiple tag bits. Thus, information from the ambient illuminator does not need to be estimated (for analog ambient illuminator) or detected (for digital ambient illuminator), as long as the sum in Eq. (17) remains constant throughout the tag-backscattered packet. Setting:

$$\gamma=\frac{1}{2}\hat{m}_{\mathrm{tag}}\,\lambda_{\mathrm{ac}}\,\mathrm{e}^{-\mathrm{j}\hat{\theta}_{\mathrm{tag}}}, \tag{18}$$

denoting $\mathbf{r}=\begin{bmatrix}r^+ & r^-\end{bmatrix}^T$ and assuming knowledge of γ and Φ_{t},

$$\begin{aligned}\mathbf{r}|\mathrm{H}_0&\sim\mathcal{CN}\left(\mathbf{0}_2,L\sigma_n^2\mathbf{I}_2\right),\\ \mathbf{r}|\mathrm{H}_1,\gamma,\Phi_{\mathrm{t}}&\sim\mathcal{CN}\left(\mu_{\mathbf{r}},L\sigma_n^2\mathbf{I}_2\right),\end{aligned} \tag{19}$$

with:

$$\mu_{\mathbf{r}}=\gamma\begin{bmatrix}\mathrm{e}^{\mathrm{j}\Phi_{\mathrm{t}}} & \mathrm{e}^{-\mathrm{j}\Phi_{\mathrm{t}}}\end{bmatrix}^T. \tag{20}$$

[2]Channel coherence time spans a limited number of bits, i.e $T_{\mathrm{coh}}\approx N_{\mathrm{pack}}\,L\,T_{\mathrm{s}}=N_{\mathrm{pack}}\,T_{\mathrm{bit}}$.

D. Coherent Detection

Given perfect information about parameters γ and Φ_{t}, the symbol-by-symbol BER-optimal ML detector is given by:

$$\mathcal{L}\left(\mathbf{r}\right)=\frac{\mathsf{f}_{\mathbf{r}|\mathrm{H}_1,\gamma,\Phi_{\mathrm{t}}}\left(\mathbf{r}|\mathrm{H}_1,\gamma,\Phi_{\mathrm{t}}\right)}{\mathsf{f}_{\mathbf{r}|\mathrm{H}_0}\left(\mathbf{r}|\mathrm{H}_0\right)}\overset{\mathrm{H}_1}{\geq}1, \tag{21}$$

where $\mathsf{f}(\cdot)$ stands for probability density function; according to Eq. (19), the above is simplified to:

$$||\mathbf{r}-\mu_{\mathbf{r}}||_2^2\overset{\mathrm{H}_1}{\leq}||\mathbf{r}||_2^2\Leftrightarrow\Re\left\{\mathbf{r}^H\mu_{\mathbf{r}}\right\}\overset{\mathrm{H}_1}{\geq}|\gamma|^2. \tag{22}$$

It can be observed that in cases (e.g., standard BPSK) where the sum of Eq. (17) is approximately zero, the detector will fail.[3] For such cases, the scheme presented in Sec. IV can be utilized.

E. Probability of Error

If the channel fading parameters are Rayleigh distributed, it can be easily shown that the total probability of error is given by:

$$\begin{aligned}\Pr\left(e\right)&=\mathop{\mathbb{E}}_{|\gamma|}\left[\Pr\left(e\middle||\gamma|\right)\right]=\mathop{\mathbb{E}}_{|\gamma|}\left[\mathsf{Q}\left(\frac{|\gamma|}{\sqrt{L\sigma_n^2}}\right)\right]\\&\overset{\text{(a)}}{=}\frac{1}{2}-\frac{\sqrt{\pi}}{4}U\left(\frac{1}{2},0,\frac{2}{\overline{SNR}}\right),\end{aligned} \tag{23}$$

where $U(\cdot,\cdot,\cdot)$ is the confluent hypergeometric function [33, eq. (13.4.4)]. Point (a) involves calculating the expectation of $\mathsf{Q}\left(\frac{|\gamma|}{\sqrt{L\sigma_n^2}}\right)$ over the product of Rayleigh distributed r.vs $a_{\mathrm{CT}},a_{\mathrm{TR}}$. Analytical derivation of the expression can be found in [11, App. II]. $\overline{SNR}$ is given by:

$$\overline{SNR}=\frac{\mathbb{E}\left[|\gamma|^2\right]}{L\sigma_n^2}=\frac{\beta^2\mathbb{E}\left[a_{\mathrm{CT}}^2\right]\mathbb{E}\left[a_{\mathrm{TR}}^2\right]}{L\sigma_n^2}, \tag{24}$$

with:

$$\beta=\frac{1}{4}A_{\mathrm{c}}\,\mathrm{s}\,m_{\mathrm{tag}}\left|\lambda_{\mathrm{ac}}\right|. \tag{25}$$

F. Compound Channel Estimation

Parameter $\mu_{\mathbf{r}}$ is assumed constant through the transmission of N_{pack} bits. Thus, a portion of the total N_{pack} tag bits, the first N_{tr} bits, can be allocated as a training sequence for estimation of $\mu_{\mathbf{r}}$.

The output of the correlators, for a single bit, can be also written in the following form:

$$\mathbf{r}_i=s_i\mu_{\mathbf{r}}+\mathbf{n}_i=s_i\,\mathbf{I}_2\,\mu_{\mathbf{r}}+\mathbf{n}_i, \tag{26}$$

where $s_i\in\{0,1\}$ and $\mathbf{n}_i=[n^+\quad n^-]^T$. By vertically concatenating all the received vectors corresponding to the first N_{tr} bits, the vector $\mathbf{y}_{\mathrm{tr}}$ can be defined as:

$$\mathbf{y}_{\mathrm{tr}}=\begin{bmatrix}\mathbf{r}_1\\\mathbf{r}_2\\\vdots\\\mathbf{r}_{N_{\mathrm{tr}}}\end{bmatrix}=\begin{bmatrix}s_1\mathbf{I}_2\\s_2\mathbf{I}_2\\\vdots\\s_{N_{\mathrm{tr}}}\mathbf{I}_2\end{bmatrix}\mu_{\mathbf{r}}+\begin{bmatrix}\mathbf{n}_1\\\mathbf{n}_2\\\vdots\\\mathbf{n}_{N_{\mathrm{tr}}}\end{bmatrix}=\mathbf{T}\mu_{\mathbf{r}}+\tilde{\mathbf{n}}, \tag{27}$$

[3]If the sum is approximately zero, then parameter $\mu_{\mathbf{r}}$ will also be approximately zero and the detector will not work.

where matrix $\mathbf{T}$ is known to the receiver and $\tilde{\mathbf{n}}\sim\mathcal{CN}\left(\mathbf{0}_{2N_{\mathrm{tr}}},L\sigma_n^2\mathbf{I}_{2N_{\mathrm{tr}}}\right)$.

Given $\mathbf{T}$ and correlator samples $\mathbf{y}_{\mathrm{tr}}$, an estimate $\hat{\mu}_{\mathbf{r}}$ of $\mu_{\mathbf{r}}$ is given by solving the least squares problem:

$$\hat{\mu}_{\mathbf{r},\mathrm{ls}}=\arg\min_{\mu_{\mathbf{r}}\in\mathbb{C}^2}||\mathbf{y}_{\mathrm{tr}}-\mathbf{T}\mu_{\mathbf{r}}||_2^2. \tag{28}$$

Setting the gradient of Eq. (28) equal to zero, the LS-solution takes the form [34, pp. 521]:

$$\hat{\mu}_{\mathbf{r},\mathrm{ls}}=\left(\mathbf{T}^H\mathbf{T}\right)^{-1}\mathbf{T}^H\mathbf{y}_{\mathrm{tr}}. \tag{29}$$

IV. Partially Coherent S-BPSK

In the previous section a coherent ML detector was derived assuming that the structure of the ambient carrier's signal was known (constant envelope signal). In this section, a partially-coherent detector will be derived for a hybrid form of FSK-BPSK modulation, while assuming no information about the ambient carrier.

A. Modulation & Signal Model

The modulation scheme suggested in this section involves encapsulating information in the phase of the tag's switching signal. More specifically, in Eq. (6), for the duration of a single bit, it is assumed that:

$$\mathsf{x}_{\mathrm{tag}}^{\mathrm{SB},i}\left(t\right)=m_{\mathrm{dc}}\mathsf{e}^{\mathsf{j}\theta_{\mathrm{dc}}}+m_{\mathrm{tag}}\,\mathsf{e}^{\mathsf{j}\theta_{\mathrm{tag}}}\mathsf{cos}\left(2\pi F_{\mathrm{sw}}\,t+\Phi_{\mathrm{t}}+\phi_i\left(t\right)\right), \tag{30}$$

with:

$$\phi_i\left(t\right)=\begin{cases}\Phi_0, & i=0,\\ \Phi_1=\Phi_0+\Delta\phi, & i=1.\end{cases} \tag{31}$$

Tag's signal in Eq. (30) can be realized by driving the RF switch by an already BPSK modulated signal, centered at frequency F_{sw}.[4] This modulation may be termed shifted BPSK because, as will later be evident, of the frequency shift that the illuminating carrier's spectrum undergoes due to switching at F_{sw}.

Following the assumptions made in Sec. III-A *without*, however, assuming a constant envelope illumination but instead a general model for the ambient carrier's complex envelope $\mathsf{m}\left(t\right)=m_{\mathrm{ac}}\left(t\right)\mathsf{e}^{\mathsf{j}\Phi_{\mathrm{ac}}(t)}$, the signal at the reader, assuming perfect CFO correction and following Eq. (4), can be expressed as follows:

$$\begin{aligned}\mathsf{y}_i^{\mathrm{SB}}\left(t\right)&=a_{\mathrm{dr}}\mathsf{e}^{\mathsf{j}\theta_{\mathrm{dr}}}\mathsf{m}\left(t\right)+\hat{m}_{\mathrm{mod}}\mathsf{e}^{-\mathsf{j}\hat{\theta}_{\mathrm{mod}}}\\&\quad\times\mathsf{m}\left(t\right)\mathsf{cos}\left(2\pi F_{\mathrm{sw}}t+\Phi_{\mathrm{t}}+\Phi_i\right)+n\left(t\right),\end{aligned} \tag{32}$$

where the parameters are given by:

$$\begin{aligned}a_{\mathrm{dr}}\mathsf{e}^{\mathsf{j}\theta_{\mathrm{dr}}}&=\frac{1}{2}a_{\mathrm{CR}}\mathsf{e}^{-\mathsf{j}(\phi_{\mathrm{CR}}+\Delta\phi_c)}+\hat{m}_{\mathrm{d}}\mathsf{e}^{-\mathsf{j}\hat{\theta}_{\mathrm{d}}},\\\hat{m}_{\mathrm{d}}&=\frac{1}{2}\,\mathrm{s}\,a_{\mathrm{CT}}\,a_{\mathrm{TR}}\,m_{\mathrm{dc}},\\\hat{\theta}_{\mathrm{d}}&=\phi_{\mathrm{CT}}+\phi_{\mathrm{TR}}+\Delta\phi_c-\theta_{\mathrm{dc}},\end{aligned}$$

[4]As will be evident subsequently, this operation is similar to Eq. (54), only in this case, $\phi_i\left(t\right)$ is discrete and resembles phase modulation (PM) rather than FM.

$$\hat{m}_{\rm mod} = \frac{1}{2}\,{\rm s}\,a_{\rm CT}\,a_{\rm TR}\,m_{\rm tag},$$
$$\hat{\theta}_{\rm mod} = \phi_{\rm CT} + \phi_{\rm TR} + \Delta\phi_c - \theta_{\rm tag}. \tag{33}$$

Similarly to Eq. (13) is is also assumed that:

$$\mathrm{BW}\left(\mathsf{m}\left(t\right)\right) \ll F_{\rm sw}. \tag{34}$$

B. Correlators, Statistics & Partially Coherent, Uncoded Detection Rule

To aid the decision process the correlators of Eq. (14) are used utilizing, however, $\mathsf{y}_i^{\rm SB}[k] = \mathsf{y}_i^{\rm SB}(kT_{\rm s})$. In a similar manner to Sec. III-B and for the nth bit, $r_{s,n}^{+}$ output is given by:

$$\begin{aligned} r_{s,n}^{+} &= a_{\rm dr}\mathsf{e}^{\mathsf{j}\theta_{\rm dr}}\overbrace{\sum_{k=0}^{L-1}\mathsf{m}\left[k\right]\mathsf{e}^{-\mathsf{j}2\pi F_{\rm sw}kT_{\rm s}}}^{\approx 0} \\ &+ \frac{\hat{m}_{\rm mod}\mathsf{e}^{-\mathsf{j}\hat{\theta}_{\rm mod}}}{2}\mathsf{e}^{\mathsf{j}\Phi_{\rm t}}\mathsf{e}^{\mathsf{j}\Phi_{i_n}}\sum_{k=0}^{L-1}\mathsf{m}\left[k\right]\mathsf{e}^{\mathsf{j}2\pi F_{\rm sw}kT_{\rm s}}\mathsf{e}^{-\mathsf{j}2\pi F_{\rm sw}kT_{\rm s}} \\ &+ \frac{\hat{m}_{\rm mod}\mathsf{e}^{-\mathsf{j}\hat{\theta}_{\rm mod}}}{2}\mathsf{e}^{-\mathsf{j}\Phi_{\rm t}}\mathsf{e}^{-\mathsf{j}\Phi_{i_n}}\underbrace{\sum_{k=0}^{L-1}\mathsf{m}\left[k\right]\mathsf{e}^{-\mathsf{j}4\pi F_{\rm sw}kT_{\rm s}}}_{\approx 0} \\ &+ \underbrace{\sum_{k=0}^{L-1}n\left[k\right]\mathsf{e}^{-\mathsf{j}2\pi F_{\rm sw}kT_{\rm s}}}_{\triangleq n^{+}} \\ &= \gamma_{\rm s}\,\mathsf{e}^{\mathsf{j}(\Phi_{\rm t}+\Phi_{i_n})}\mu_n + n_n^{+}, \end{aligned} \tag{35}$$

where Eq. (34) was used. Calculation of $r_{{\rm s},n}^{-}$ can be performed in a similar manner. The outputs of the two correlators are summarized below:

$$\begin{aligned} r_{{\rm s},n}^{+} &= \gamma_{\rm s}\,\mathsf{e}^{\mathsf{j}(\Phi_{\rm t}+\Phi_{i_n})}\mu_n + n_n^{+}, \\ r_{{\rm s},n}^{-} &= \gamma_{\rm s}\,\mathsf{e}^{-\mathsf{j}(\Phi_{\rm t}+\Phi_{i_n})}\mu_n + n_n^{-}, \end{aligned} \tag{36}$$

where $n_n^{\pm} \sim \mathcal{CN}\left(0, \tilde{\sigma}_n^2\right)$ with $\tilde{\sigma}_n^2 = L\sigma_n^2$ and:

$$\gamma_{\rm s} = \frac{\hat{m}_{\rm mod}\mathsf{e}^{-\mathsf{j}\hat{\theta}_{\rm mod}}}{2}, \quad \mu_n = \sum_{k=0}^{L-1}\mathsf{m}\left[k\right]. \tag{37}$$

SNR is defined at the output of the correlators such that:

$$\mathrm{SNR} = \frac{{\rm s}^2\mathbb{E}\left[a_{\rm CT}^2\right]\mathbb{E}\left[a_{\rm TR}^2\right]m_{\rm mod}^2\mathbb{E}\left[|\mu_n|^2\right]}{16\tilde{\sigma}_n^2} \tag{38}$$

For nth bit $i_n \in \{0,1\}$, vector $\mathbf{r}_{{\rm s},n}$ is defined as:

$$\begin{aligned} \mathbf{r}_{{\rm s},n} &= \begin{bmatrix} r_{{\rm s},n}^{+} \\ r_{{\rm s},n}^{-} \end{bmatrix} = \tilde{\mu}_n \begin{bmatrix} \mathsf{e}^{\mathsf{j}(\Phi_{\rm t}+\Phi_{i_n})} \\ \mathsf{e}^{-\mathsf{j}(\Phi_{\rm t}+\Phi_{i_n})} \end{bmatrix} + \begin{bmatrix} n_n^{+} \\ n_n^{-} \end{bmatrix} \\ &= \tilde{\mu}_n\mathbf{x}_{i_n}(\Phi_{\rm t}) + \tilde{\mathbf{n}}_n, \end{aligned} \tag{39}$$

where $\tilde{\mathbf{n}}_n \sim \mathcal{CN}\left(\mathbf{0}_2, \tilde{\sigma}_n^2\mathbf{I}_2\right)$ and:

$$\tilde{\mu}_n = \gamma_{\rm s}\mu_n. \tag{40}$$

Thus, given perfect knowledge of $\tilde{\mu}_n$ and $\Phi_{\rm t}$, the statistical description of Eq. (39) is:

$$\mathbf{r}_{{\rm s},n}|\mathrm{H}_{i_n}, \tilde{\mu}_n, \Phi_{\rm t} \sim \mathcal{CN}\left(\tilde{\mu}_n\,\mathbf{x}_{i_n}(\Phi_{\rm t}), \tilde{\sigma}_n^2\mathbf{I}_2\right). \tag{41}$$

Thus, the pdf of $\mathbf{r}_{{\rm s},n}$ is given by [34, pp. 504]:

$$\begin{aligned} &\mathsf{f}_{\mathbf{r}_{{\rm s},n}|\mathrm{H}_{i_n},\tilde{\mu}_n,\Phi_{\rm t}}(\mathbf{r}_{{\rm s},n}|\mathrm{H}_{i_n},\tilde{\mu}_n,\Phi_{\rm t}) \\ &\qquad = \frac{1}{\pi^2\tilde{\sigma}_n^4}\mathsf{e}^{-\frac{1}{\tilde{\sigma}_n^2}||\mathbf{r}_{{\rm s},n}-\tilde{\mu}_n\,\mathbf{x}_{i_n}(\Phi_{\rm t})||_2^2}. \end{aligned} \tag{42}$$

If variables $\tilde{\mu}_n$, $\Phi_{\rm t}$ were known, the BER-optimal detector, given equiprobable signaling, would be the maximum likelihood (ML) detector. $\Phi_{\rm t}$, as stated earlier is considered random, but constant through the duration of a packet, thus it is possible to estimate it using a known training sequence within the packet. Unlike $\Phi_{\rm t}$, $\tilde{\mu}_n$ contains information from the ambient carrier[5] and in the general case, varies between successive bits. Thus, training sequence can not be used, and coherent detection can not be applied. To overcome this problem, generalized likelihood ratio test (GLRT) will be utilized in the same way as in [8], while (in contrast to [8]) considering a modulated carrier and a different modulation scheme at the tag. $\tilde{\mu}_n$ will be considered as an unknown parameter and maximization of Eq. (42) over that parameter will be performed. Thus, using the above, the log decision rule becomes [35, pp. 200]:

$$\mathcal{L}_G\left(\mathbf{r}_{{\rm s},n}\right) = \frac{\max\limits_{\tilde{\mu}_n}\ln\left[\mathsf{f}_{\mathbf{r}_{{\rm s},n}|\mathrm{H}_1,\tilde{\mu}_n,\Phi_{\rm t}}(\mathbf{r}_{{\rm s},n}|\mathrm{H}_1,\tilde{\mu}_n,\Phi_{\rm t})\right]}{\max\limits_{\tilde{\mu}_n}\ln\left[\mathsf{f}_{\mathbf{r}_{{\rm s},n}|\mathrm{H}_0,\tilde{\mu}_n,\Phi_{\rm t}}(\mathbf{r}_{{\rm s},n}|\mathrm{H}_0,\tilde{\mu}_n,\Phi_{\rm t})\right]} \underset{\mathrm{H}_0}{\overset{\mathrm{H}_1}{\gtrless}} 1. \tag{43}$$

It can be easily shown (see Appendix) that the aforementioned decision rule can be simplified to the following expression:

$$\begin{aligned} &\Re\left\{\left(r_{{\rm s},n}^{+}\right)^{*}\left(r_{{\rm s},n}^{-}\right)\mathsf{e}^{\mathsf{j}2(\Phi_{\rm t}+\Phi_1)}\right\} \\ &\quad \overset{\mathrm{H}_1}{\geq} \Re\left\{\left(r_{{\rm s},n}^{+}\right)^{*}\left(r_{{\rm s},n}^{-}\right)\mathsf{e}^{\mathsf{j}2(\Phi_{\rm t}+\Phi_0)}\right\} \\ &\quad \Leftrightarrow \Re\left\{\mathsf{e}^{\mathsf{j}\theta_{{\rm p},n}}\mathsf{e}^{\mathsf{j}2(\Phi_{\rm t}+\Phi_0)}\left(\mathsf{e}^{\mathsf{j}2\Delta\phi}-1\right)\right\} \overset{\mathrm{H}_1}{\geq} 0, \end{aligned} \tag{44}$$

where $|r_{{\rm p},n}|\mathsf{e}^{\mathsf{j}\theta_{{\rm p},n}} = \left(r_{{\rm s},n}^{+}\right)^{*}\left(r_{{\rm s},n}^{-}\right)$. If $\Phi_0 = 0$ and $\Delta\phi = \frac{\pi}{2}$ are chosen, the decision rule of Eq. (44) can be expressed as:

$$\cos\left(2\Phi_{\rm t} + \theta_{{\rm p},n}\right) \overset{\mathrm{H}_1}{\leq} 0, \tag{45}$$

The derived detector of Eq. (45) demonstrates that given $\Phi_{\rm t}$, *no knowledge* regarding the ambient carrier is necessary to perform detection.

C. Estimation of Φ_t

In order for the detector of Eq. (45) to decide, $\Phi_{\rm t}$ is necessary. A heuristic estimation scheme utilizing a number of training bits at the start of the packet will be used. Assuming that a single 0-valued training bit is used and ignoring the noise, the noiseless output of the correlators is given by:

$$r_1^{+} = \tilde{\mu}_1\,\mathsf{e}^{\mathsf{j}\Phi_{\rm t}}, \quad r_1^{-} = \tilde{\mu}_1\,\mathsf{e}^{-\mathsf{j}\Phi_{\rm t}}. \tag{46}$$

[5]Additionally $\tilde{\mu}_n$ contains wireless channel and tag related parameters which can be considered constant for the duration of a packet.

The product of the two correlators is considered which results to $r_1^+ \left(r_1^-\right)^* = |\tilde{\mu}_1|^2 \mathrm{e}^{\mathrm{j}2\Phi_\mathrm{t}}$ and $\widehat{\Phi}_\mathrm{t} = \frac{\angle r_1^+ \left(r_1^-\right)^*}{2}$. In the case where N_tr, zero-valued, training bits are available, two $1 \times N_\mathrm{tr}$ vectors are constructed: $\mathbf{r}_{1:N_\mathrm{tr}}^+ = \left[r_1^+ \; r_2^+ \; \ldots \; r_{N_\mathrm{tr}}^+\right]$ and $\mathbf{r}_{1:N_\mathrm{tr}}^- = \left[r_1^- \; r_2^- \; \ldots \; r_{N_\mathrm{tr}}^-\right]$. Then the estimate of Φ_t is evaluated as $\widehat{\Phi}_\mathrm{t} = \frac{\angle \mathbf{r}_{1:N_\mathrm{tr}}^+ \left(\mathbf{r}_{1:N_\mathrm{tr}}^-\right)^H}{2}$.

D. Coded Sequence Detection

The tag is assumed to utilize an error correcting code $\mathcal{C}$. Each sequence of k bits is mapped by the code to a new, coded sequence $\mathbf{c} \in \mathcal{C}$ of N_c bits. When such coded transmission is utilized, in the same way as presented in [8], the following decision rule can be utilized:

$$\widehat{\mathbf{c}} = \arg\max_{\mathbf{c}\in\mathcal{C}} \left\{ \max_{\mu_\mathbf{c}\in\mathbb{C}^{N_\mathrm{c}}} \ln\left[\mathsf{f}_{\mathbf{r}_{\mathrm{s},1:N_\mathrm{c}}|\mathbf{c},\mu_\mathbf{c},\Phi_\mathrm{t}}(\mathbf{r}_{\mathrm{s},1:N_\mathrm{c}}|\mathbf{c},\mu_\mathbf{c},\Phi_\mathrm{t})\right] \right\}, \tag{47}$$

where $\mu_\mathbf{c} = [\tilde{\mu}_1 \; \tilde{\mu}_2 \; \ldots \; \tilde{\mu}_{N_\mathrm{c}}]^T$ and:

$$\mathbf{r}_{\mathrm{s},1:N_\mathrm{c}} = \begin{bmatrix} \mathbf{r}_{\mathrm{s},1} \\ \mathbf{r}_{\mathrm{s},2} \\ \vdots \\ \mathbf{r}_{\mathrm{s},N_\mathrm{c}} \end{bmatrix} = \begin{bmatrix} \tilde{\mu}_1 \, \mathbf{x}_1(\Phi_\mathrm{t}) \\ \tilde{\mu}_2 \, \mathbf{x}_2(\Phi_\mathrm{t}) \\ \vdots \\ \tilde{\mu}_{N_\mathrm{c}} \, \mathbf{x}_{N_\mathrm{c}}(\Phi_\mathrm{t}) \end{bmatrix} + \begin{bmatrix} \tilde{\mathbf{n}}_1 \\ \tilde{\mathbf{n}}_2 \\ \vdots \\ \tilde{\mathbf{n}}_{N_\mathrm{c}} \end{bmatrix}. \tag{48}$$

Assuming that variables $\tilde{\mu}_1 \ldots \tilde{\mu}_{N_\mathrm{c}}$ are independent and exploiting the conditional independence of each $\mathbf{r}_{\mathrm{s},n}$ (given $\mathbf{c}$, $\tilde{\mu}_n$ and Φ_t) the right-most maximization in Eq. (47) can be expressed as follows:

$$\begin{aligned} &\max_{\mu_\mathbf{c}\in\mathbb{C}^{N_\mathrm{c}}} \ln\left[\mathsf{f}_{\mathbf{r}_{\mathrm{s},1:N_\mathrm{c}}|\mathbf{c},\mu_\mathbf{c},\Phi_\mathrm{t}}(\mathbf{r}_{\mathrm{s},1:N_\mathrm{c}}|\mathbf{c},\mu_\mathbf{c},\Phi_\mathrm{t})\right] \\ &= \sum_{n=1}^{N_\mathrm{c}} \max_{\tilde{\mu}_n} \ln\left[\mathsf{f}_{\mathbf{r}_{\mathrm{s},n}|\mathrm{H}_{c_n},\tilde{\mu}_n,\Phi_\mathrm{t}}(\mathbf{r}_{\mathrm{s},n}|\mathrm{H}_{c_n},\tilde{\mu}_n,\Phi_\mathrm{t})\right] \\ &\overset{\text{(a)}}{=} \sum_{n=1}^{N_\mathrm{c}} 2\ln\left(\frac{1}{\pi\tilde{\sigma}_n^2}\right) - \frac{1}{2\tilde{\sigma}_n^2}||\mathbf{r}_{\mathrm{s},n}||_2^2 \\ &\quad + \frac{1}{\tilde{\sigma}_n^2}\Re\left\{\left(r_{\mathrm{s},n}^+\right)^* \left(r_{\mathrm{s},n}^-\right) \mathrm{e}^{\mathrm{j}2(\Phi_\mathrm{t}+\Phi_{c_n})}\right\}, \end{aligned} \tag{49}$$

where in (a), results from Appendix were utilized. Following the same method as in [8, Sec. III-C], Eq.(49) can be expressed as follows:

$$\begin{aligned} &\sum_{n=1}^{N_\mathrm{c}} \max_{\tilde{\mu}_n} \ln\left[\mathsf{f}_{\mathbf{r}_{\mathrm{s},n}|\mathrm{H}_1,\tilde{\mu}_n,\Phi_\mathrm{t}}(\mathbf{r}_{\mathrm{s},n}|\mathrm{H}_{c_n},\tilde{\mu}_n,\Phi_\mathrm{t})\right] \\ &= \sum_{n=1}^{N_\mathrm{c}} K^{(n)} + (1-c_n)\,\Lambda_0^{(n)} + c_n\Lambda_1^{(n)} \\ &= \sum_{n=1}^{N_\mathrm{c}} K^{(n)} + \Lambda_0^{(n)} + c_n\left(\Lambda_1^{(n)} - \Lambda_0^{(n)}\right), \end{aligned} \tag{50}$$

where $K^{(n)} = 2\ln\left(\frac{1}{\pi\tilde{\sigma}_n^2} - \frac{1}{2\tilde{\sigma}_n^2}||\mathbf{r}_{\mathrm{s},n}||_2^2\right)$ and:

$$\Lambda_{c_n}^{(n)} = \frac{1}{\tilde{\sigma}_n^2}\Re\left\{\left(r_{\mathrm{s},n}^+\right)^* \left(r_{\mathrm{s},n}^-\right) \mathrm{e}^{\mathrm{j}2(\Phi_\mathrm{t}+\Phi_{c_n})}\right\}. \tag{51}$$

Neglecting the terms that do not affect the left-most maximization in Eq. (47), assuming $\Phi_0 = 0$, $\Delta\phi = \frac{\pi}{2}$ and exploiting Eq. (50), after calculations, the decision rule of Eq. (47) becomes:

$$\widehat{\mathbf{c}} = \arg\max_{\mathbf{c}\in\mathcal{C}} \sum_{n=1}^{N_\mathrm{c}} w_n c_n, \tag{52}$$

where $w_n = -|r_{\mathrm{p},n}|\cos\left(2\Phi_\mathrm{t} + \theta_{p,n}\right)$ and $|r_{\mathrm{p},n}|\mathrm{e}^{\mathrm{j}\theta_{\mathrm{p},n}} = \left(r_{\mathrm{s},n}^+\right)^* \left(r_{\mathrm{s},n}^-\right)$.

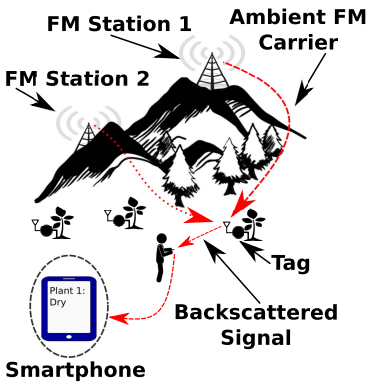

Fig. 3. Application of FM remodulation with backscatter.

V. FM Remodulation

A. FM Remodulation Principle

Ambient RF illumination from FM radio stations is considered. FM radio stations utilize wideband frequency modulation (FM), thus the passband representation of Eq. (2) is given by [26]:

$$\mathrm{c}_s(t) = \overbrace{A_s}^{m_\mathrm{ac}(t)} \cos(2\pi F_s t + \overbrace{2\pi k_\mathrm{st}\int_0^t \phi_s(\tau)\,d\tau}^{\Phi_\mathrm{ac}(t)}), \tag{53}$$

where A_s, F_s is the carrier amplitude and center frequency, respectively and k_st is the modulator's frequency sensitivity, measured in Hz/V. FM modulation index is given by $\beta_s = \Delta f_{\max}/W = k_\mathrm{st}\max|\phi_s(t)|/W$, where W is the bandwidth of $\phi_s(t)$. If an FM radio station is considered, $\phi_s(t)$ includes station's audio information plus any additional digital information about the station (radio data system-RDS), if supported.

If in Eq. (6), $\mathrm{x}_\mathrm{tag}^i(t)$ admits the following form[6]:

$$\mathrm{x}_\mathrm{tag}^i(t) \equiv \mathrm{x}_\mathrm{tag}^\mathrm{FM}(t) = A_\mathrm{sw}\cos(2\pi F_\mathrm{sw} t + \overbrace{2\pi k_\mathrm{t}\int_0^t \mu(\tau)\,d\tau}^{\phi_i(t)}), \tag{54}$$

which means that $\mu(t)$ modulates the fundamental frequency of the square wave driving the RF switch and the illuminating carrier is a *modulated* signal from an FM radio station (Eq. (53)), then the tag-backscattered signal is given by[6]:

$$\begin{aligned} \mathrm{y}_\mathrm{bs}(t) &= \mathrm{s}\,\mathrm{c}_s(t)\,\mathrm{x}_\mathrm{tag}^\mathrm{FM}(t) \\ &= \frac{\gamma_s}{2}\cos\left(2\pi\left(F_s + F_{sw}\right)t + \phi_d^t + \mu_d^t\right) \\ &\quad + \frac{\gamma_s}{2}\cos\left(2\pi\left(F_s - F_{sw}\right)t + \phi_d^t - \mu_d^t\right) \end{aligned} \tag{55}$$

[6]Tag related parameters, random phase Φ_t as well as wireless channel parameters were omitted for ease of exposition. The direct path is omitted due to the nature of the FM receiver, which tunes to a specific band.

where $\gamma_s = \mathrm{s}\, A_s\, A_{\mathrm{sw}}$, $\phi_{\mathrm{d}}^t = 2\pi k_{\mathrm{st}} \int_0^t \phi_s(\tau)\, d\tau$ and $\mu_{\mathrm{d}}^t = 2\pi k_{\mathrm{t}} \int_0^t \mu(\tau)\, d\tau$. Eq. (55) offers the sum of two FM signals at $F_s \pm F_{\mathrm{sw}}$, since their instantaneous frequency depends on $\phi_s(t) \pm \mu(t)$. Thus, backscattering results to FM signaling when the illuminating signal is FM and the switching signal is also FM.

The FM remodulation principle observed above means that any conventional FM radio receiver, tuned at either of $F_s \pm F_{\mathrm{sw}}$, can demodulate the backscattered signal, as long as the following conditions hold:

- $\mu(t)$ bandwidth is limited to the audible spectrum (20 Hz to 20 kHz) or up to the maximum frequency of 53 kHz (assuming stereo FM reception) or slightly above (RDS band).
- At least one of $F_s \pm F_{\mathrm{sw}}$ falls within the FM radio frequency band (88 MHz to 108 MHz).
- Audio level of the backscattered demodulated tag's signal (given that it's limited to the audible spectrum) is above a required threshold for successful FM reception.

In this work, sensor's $\mu(t)$ is limited in the audible spectrum, potentially amenable to interference from FM station's $\phi_s(t)$, while $k_{\mathrm{t}} \neq k_{\mathrm{st}}$. To reduce interference from the FM station signal on the tag backscattered signal, the frequency band of $\mu(t)$ may be placed on areas that are not occupied by frequency components of $\phi_s(t)$. For example, if the chosen FM radio station has only voice content, $\mu(t)$ can be designed to occupy a higher frequency band. Additionally, simulations and experiments have shown that by increasing the frequency deviation of the switching signal (up to a certain value, so that the FM threshold phenomenon does not kick in), higher audio levels of $\mu(t)$ are offered compared to interference. Such method does not eliminate interference but reduces its effect.

B. Effect of Noise

An FM receiver is considered tuned at $F_{\mathrm{bs}} = F_s + F_{\mathrm{sw}}$. The backscattered signal appearing at that frequency is given by:

$$\mathrm{y_{bu}}(t) = \gamma_{\mathrm{bs}} \cos\left(2\pi F_{\mathrm{bs}} t + \phi_{\mathrm{d}}^t + \mu_{\mathrm{d}}^t\right) + \mathsf{n}(t), \tag{56}$$

where $\gamma_{\mathrm{bs}} = \frac{\gamma_s}{2}$ and $\mathsf{n}(t)$ zero-mean, wide sense stationary (WSS) Gaussian process. In order to recover $\mu(t)$ (and $\phi_s(t)$, which acts as interference to $\mu(t)$) FM receiver down-converts the received signal, extracts the phase of the complex envelope and then derivates the result. SNR at the input of the receiver can be defined as:

$$\mathrm{SNR} = \frac{\gamma_{\mathrm{bs}}^2/2}{\mathbb{E}\left[\mathsf{n}^2(t)\right]}. \tag{57}$$

Theorem 1: Assuming wideband FM operation, $\mu(t)$ modeling a deterministic audio tone and $\phi_s(t)$ modeled as a WSS Gaussian process, the SINR, with respect to tag's signal, at the output of the FM receiver is given by:

$$SINR \approx \frac{k_t^2\, \mathbb{E}\left[\mu^2(t)\right]}{k_{st}^2\, \mathbb{E}\left[\phi_s^2(t)\right] + \frac{2\, N_0 W_m^3}{3\gamma_{\mathrm{bs}}^2} + 8\pi^2\, W_{\mathrm{m}} \widehat{\delta f}_{\mathrm{s}} \mathsf{e}^{-SNR}}, \tag{58}$$

where N_0 is the power spectral density of the noise at the input of the receiver, W_m is the bandwidth of the signal at the output of the FM receiver and $\widehat{\delta f}_{\mathrm{s}}$ is an upper bound for the average of the absolute frequency deviation:

$$\overline{|\delta f|} \leq k_{\mathrm{t}} \overline{|\mu(t)|} + k_{\mathrm{st}} \overline{|\phi_s(t)|} = \frac{2k_{\mathrm{t}}}{\pi} + \sqrt{\frac{2}{\pi}} k_{\mathrm{st}} \sqrt{P_{st}} \triangleq \widehat{\delta f}_{\mathrm{s}}. \tag{59}$$

When operating at the high SNR regime, i.e when SNR ≥ 10 dB, term $\mathsf{e}^{-\mathrm{SNR}}$ can be assumed zero and Eq. (58) offers the SINR at the output of the receiver (FM in high-SNR regime). When SNR < 10 dB, term $8\pi^2\, W_{\mathrm{m}} \widehat{\delta f}_{\mathrm{s}} \mathsf{e}^{-\mathrm{SNR}}$ cannot be neglected and the above SINR is an approximation at the receiver's output. Assuming as input to the receiver the backscattered/FM remodulated signal of Eq. (56), modeling $\phi_s(t)$ as a WSS Gaussian process and $\mu(t)$ as an (deterministic) audio tone and following classic FM analysis [25]–[27], based on the aforementioned model, the above theorem can be derived. Following FM analysis,[7] a model for the signal at the output of a conventional FM receiver is acquired along with the statistics of the noise affecting it. Thus, having derived the model, an expression for the attained SINR can be easily obtained. Detailed proof of the aforementioned theorem can be found in [36] (omitted here due to space constraints).

C. Analog Tag Implementation

The basic tag/system idea is to design two oscillators, with the first producing sensor's modulating signal $\mu(t)$ (1st modulation level) and the second be driven by the first (2nd modulation level), in order to produce the FM tag signal (according to Eq. (54)) to be scattered back. A capacitive C_s or resistive R_s sensing element is assumed, connected to the first oscillator, as shown in Fig. 4-left. In principle, any capacitive or resistive sensing element can be utilized, as explained below. Experiments have been conducted with two different capacitive sensing elements, one for soil moisture and another for air humidity.

1) Circuit Design: The function of the first oscillator is to translate the value of a measured quantity to the fundamental frequency of a periodic wave $\mu(t)$. To implement such functionality an ultra-low power variant of the 555 timer was utilized. The soil moisture sensing element, part of the sensor in [7] was used. Tests were also performed using a HCH-1000 humidity sensing element, part of the sensor in [5].

A Silicon Laboratories TS3002 timer, configured as a voltage controlled oscillator (VCO) (Fig. 4-left), implements oscillator B. VCO's control voltage is set to $\mu(t)$, and thus, VCO's output is a signal whose instantaneous frequency is controlled by $\mu(t)$. The maximum and minimum levels of $\mu(t)$ define the maximum and minimum frequency values produced by the VCO. The last, produces an FM signal with specific frequency limits/deviation; this is accomplished by scaling performed on $\mu(t)$ by a signal conditioning/resistor network block (Fig. 4-left). ADG919 by Analog Devices was chosen to perform RF switching due to its ultra-low power consumption ($< 1\mu$A).

[7] Considering the information signal to be the superposition of the tag's $\mu(t)$ and station's $\phi_s(t)$.

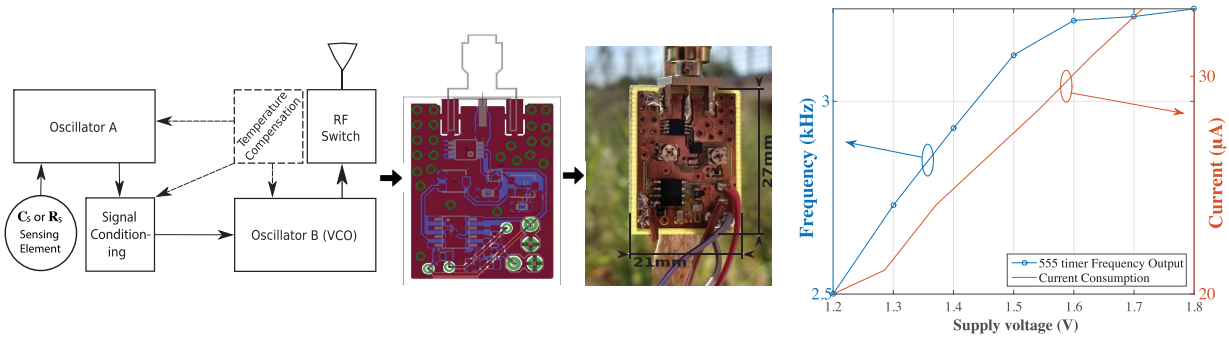

Fig. 4. Tag implementation & current consumption/frequency drift vs supply voltage.

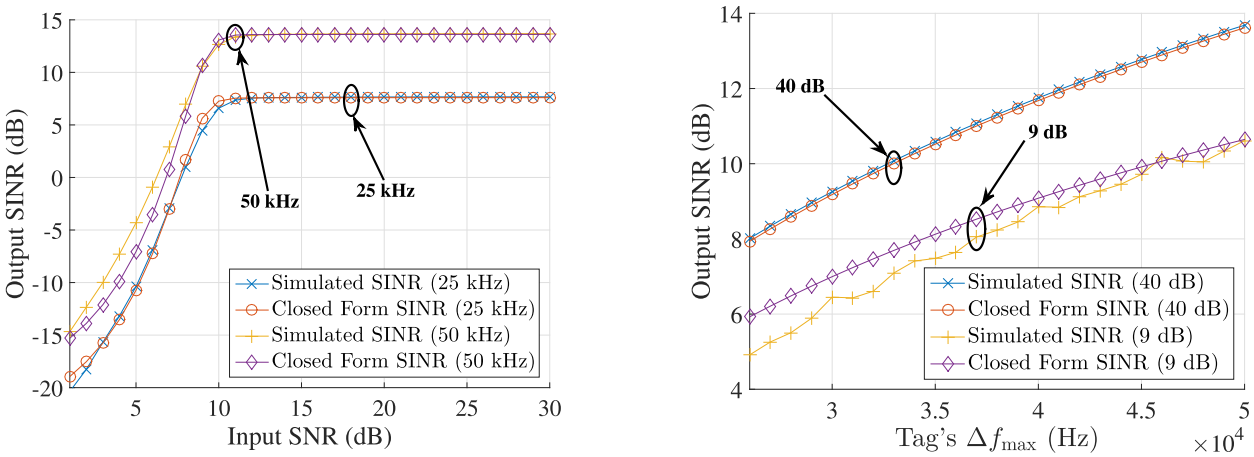

Fig. 5. (Left) Output SINR vs input SNR for 2 different tag maximum deviation settings. (Right) Output SINR vs tag's maximum frequency deviation $\Delta f_{\max} = k_{\mathrm{t}} \max |\mu(t)| = k_{\mathrm{t}}$ for input SNR of 40 and 9 dB. The station's maximum deviation was 35 kHz and $\phi_s(t)$ a recorded sound clip.

2) Power Consumption & Supply: For fixed sensing capacitor value (sensor dry), Fig. 4-right offers the overall current consumption of the tag, as a function of supply voltage; it is shown that the system is capable of achieving < 20 μA @ 1.2 V, which results to **24 μW** of power consumption. Using a standard capacitor as sensing element, the dependence of Oscillator's A output frequency is depicted in Fig. 4-right. Clearly, voltage regulation is necessary.

The tag was tested in continuous operation scenarios using either a small (31×31 mm) solar panel or a battery comprised of two lemons. Duty cycled operation was tested using a single photodiode and a boost converter circuit.

3) Receiver: As stated in Sec. V-A, any conventional FM radio receiver can be used, provided that $\mu(t)$ is audible. FM radio is a common feature among many (smart)phones. Exploiting selection by tunning at the FM station that offers the strongest demodulated tag's tone, the sensor's value can be extracted by frequency estimation of the tag's received audible tone. Tag's signal can be recovered by a computer using either an FM radio connected to audio input or an SDR (e.g., RTL-SDR).

Second, a dedicated carrier, other than the ambient FM signals, can illuminate the tag. The tag is indifferent with respect to the carrier used and an appropriately configured SDR can be used to recover tag's information. In the aforementioned scenarios, tag can potentially be powered via RF harvesting. In the phone case, harvesting can be done from phone's cellular transmissions, while in the dedicated illumination case from the carrier itself.

VI. Numerical Results

A. Simulation Results

1) FM Remodulation: Eq. (56) was modeled with $F_{\mathrm{bs}} = 2$ MHz and γ_b chosen so that the "transmission power" of the tag be equal to -80 dBm. Noise level P_n, was varied in order to obtain different input SNR values. Noise power spectral density N_0 was calculated as $P_n = \int_{-\frac{B}{2}}^{\frac{B}{2}} N_0 df = N_0 B \Leftrightarrow N_0 = \frac{P_n}{B}$. Signal $\phi_s(t)$ was a 6 second recorded clip from a local radio station. Tag's information signal was modeled as $\mu(t) = -\sin(2\pi F_{\mathrm{sens}} t)$ with $F_{\mathrm{sens}} = 3.2$ kHz. A message bandwidth of $W_{\mathrm{m}} = 50$ kHz was considered. The final signal model was sampled at $F_s = 10$ MHz. No band selection filter was used. Thus, in order to calculate N_0, the value used for B was $B = 2\ B/2 = F_s$. Then the receiver was implemented as described in Sec. V-B. Closed-form SINR was defined as per Eq. (58). Simulated SINR was returned by MATLAB's snr function [37] using as input the receiver's processed (output) signal.

Fig. 5-Left offers the behavior of the receiver's output SINR when the input SNR was varied. There are two points worth of attention in this plot. Firstly, it can be seen that

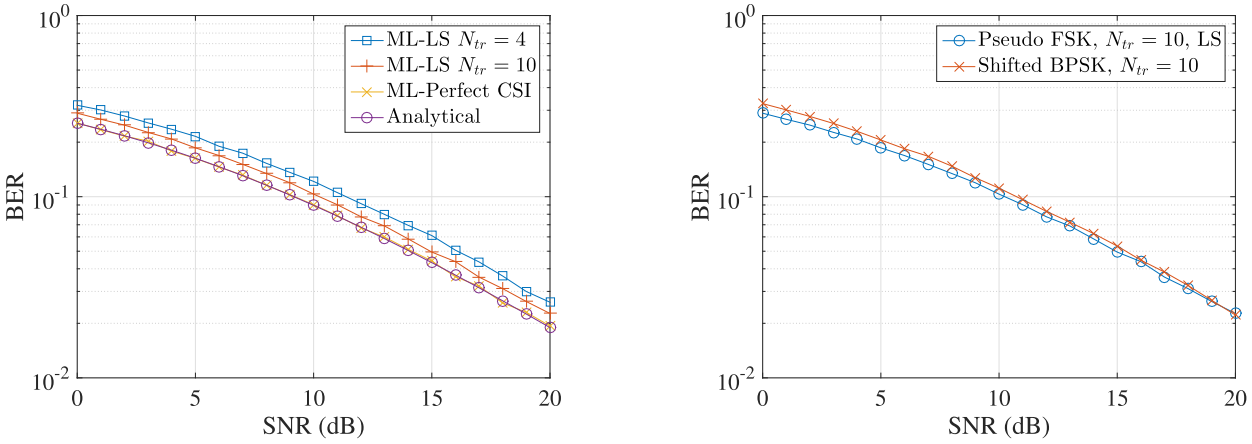

Fig. 6. (Left) BER of P-FSK scheme vs average received SNR for Rayleigh fading. (Right) Comparison of the suggested digital schemes.

around 10 dB the threshold phenomenon kicks in. Below that $\sim$ 10 dB threshold, the output SINR drops rapidly with respect to input SNR. This observation shows intuitively that, the larger the number of stations available to choose from, the better the chances of attaining drastically better performance with respect to output SINR. Secondly, it can be observed that above the threshold, the output SINR is almost constant with respect to input SNR. This comes in agreement with the experimental measurements in Fig. 9, where for small tag-2-smartphone distances (i.e higher input SNR), up to $\sim$ 8 meters, the ouput audio level is constant. It was observed through simulations that this behavior is due to the presence of FM station's $\phi_s(t)$ signal. When station's signal was omitted, a common linear[8] increace in output S(I)NR with respect to input SNR was observed (for high input SNR).

Fig. 5-Right shows dependence of output SINR on tag's maximum frequency deviation (i.e on k_{t}), with fixed FM station's maximum deviation. The simulation verifies the experimental tests, where by increasing the maximum frequency deviation of the tag's VCO, higher audio levels (for the tag's signal) at the output of the receiver were observed. The effect can be also observed in Fig. 5-Left, where for higher maximum frequency deviation, a significant increase in output SINR is attained, for a fixed input SNR value. It must be noted, that no threshold phenomena were observed in simulations. That is due to the fixed noise bandwidth and the small values of the overall maximum frequency deviation of Eq. (56) (compared to that bandwidth). It should be also noted that the small gap between simulated results and closed-form expressions for the low-SNR case are due to the approximations of the analysis in the low-SNR regime [25], [36].

2) P-FSK: Channel coefficients were created such that $h_{\mathrm{p}} \sim \mathcal{CN}(0,1)$, $\mathrm{p} \in \{\mathrm{CR}, \mathrm{CT}, \mathrm{TR}\}$, corresponding to Rayleigh fading parameters a_{p} with $\mathbb{E}\left[a_{\mathrm{p}}^2\right] = 1$. Bitrate and sampling rate were set to $R = 1$ kbps and $F_{\mathrm{s}} = 2$ MHz, respectively, resulting to $L = 2000$. Packet size was fixed at $N_{\mathrm{pack}} = 100$ bits. Tag RF-related parameters were set to $\Gamma_0 = 1$, $\Gamma_1 = -1$, $A_{\mathrm{s}} = 0.6047 + \mathrm{j}0.5042$ and scattering efficiency of $\mathrm{s} = \sqrt{0.1}$ was assumed. Station's received RF power was set to $P_{\mathrm{c}} = -40$ dBm. Stations' information signal $\phi(t)$ was modeled as a zero mean Gaussian process, which is in compliance with modeling performed for FM analysis (see e.g., [26]); phase samples $\phi[k]$ are IID and are drawn from $\mathcal{N}(0, P_\phi)$, where P_ϕ is the average power of signal $\phi(t)$, set to $P_\phi = 1$. Utilizing the previous assumption, λ_{ac} becomes:

$$\lambda_{\mathrm{ac}} = L\mathbb{E}\left[\mathrm{e}^{\mathrm{j}\phi}\right] = LM_\phi(\mathrm{j}) = L\mathrm{e}^{-\frac{P_\phi}{2}}, \tag{60}$$

where $M_\phi(\nu\mathrm{j}) = \mathrm{e}^{-\frac{\nu^2 P_\phi}{2}}$ is the characteristic function of ϕ [38, pp. 25]. Monte Carlo experiments were performed using a total of 1.5 million bits per $\overline{SNR}$ value.

Fig. 6-Left quantifies the BER performance of the detector. It can be observed that the analytical BER of Eq. (23) matches simulation results of Eq. (22), under perfect channel state information (CSI). It can also be seen that under perfect CSI compared to $N_{\mathrm{tr}} = 4$ ($N_{\mathrm{data}} = 96$), the detector offers ~ 2 dB better performance than using the estimated channel. Allocating more bits for channel estimation purposes, lowers the difference between the ML-detector with perfect CSI and the ML detector using the channel estimate. Specifically, for the chosen values and for 6 more training bits (6 less data bits/packet) the difference drops from ~ 2 dB to ~ 1 dB.

3) S-BPSK: The same parameters as with Sec. VI-A.2 were used (except for $R = 0.5$ kbps). Due to the detector being illumination-agnostic, in the context of simulations it was assumed that $\mathsf{m}[k] \sim \mathcal{CN}(0, P_{\mathrm{a}})$ with $P_{\mathrm{a}} = 1$ and the SNR was defined as per Eq. (38), with $\mathbb{E}\left[|\mu_n|^2\right] = LP_{\mathrm{a}}$. It is noted that the derivation of S-BPSK detectors does not assume any information (besides assumption of Eq. (34)) regarding the ambient carrier. Complex normal illumination is considered only for simulation purposes to ensure an independently-varying ambient signal. The detector has also been successfully tested with the illuminator employing MSK, BPSK, QPSK and FM modulations. For the coded case, BCH code was used with codeword length $N_{\mathrm{c}} = 31$ and uncoded word length $k = 11$. The wireless channel parameters were considered constant for the duration of N_{c} coded bits.

Fig. 7 demonstrates the performance of the detector in Eq. (45), compared to ML detector utilizing full (and perfect) information regarding $\tilde{\mu}_n \mathbf{x}_{i_n}(\Phi_{\mathrm{t}})$. The partially coherent detector is also evaluated for the following cases:

[8]In the dB domain.

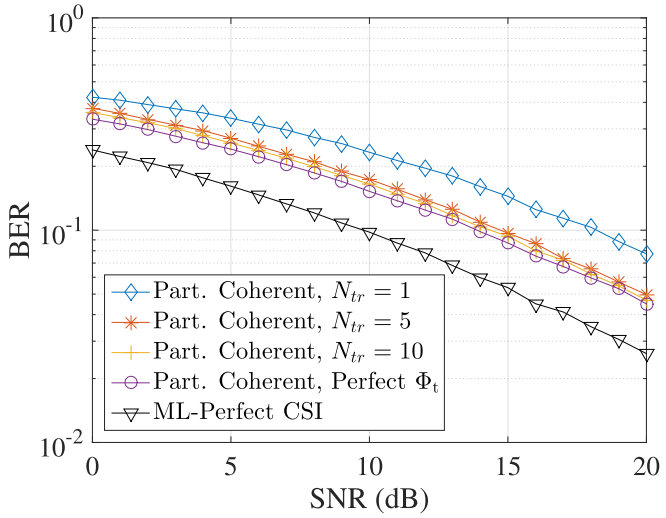

Fig. 7. BER vs average received SNR for the S-BPSK/partially coherent scheme, under Rayleigh fading, while $\Phi_0 = 0$ and $\Phi_1 = \frac{\pi}{2}$.

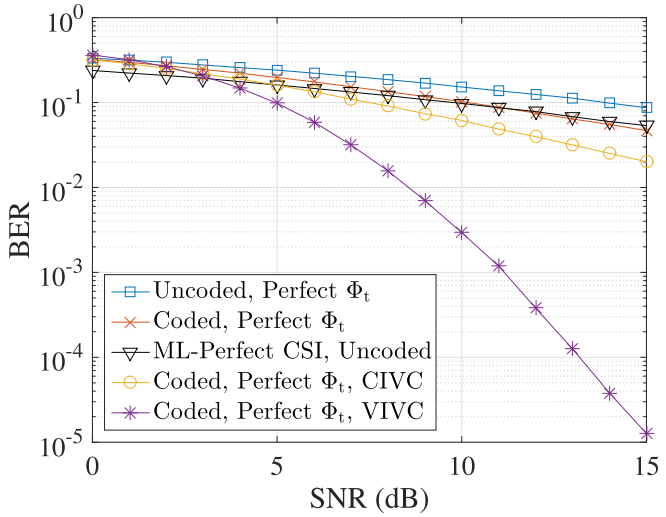

Fig. 8. BER vs average received SNR utilizing $(31, 11)$ BCH coding under Rayleigh fading for the partially coherent scheme with $\Phi_0 = 0$ and $\Phi_1 = \frac{\pi}{2}$. CIVC denotes the case of constant (for the duration of the packet) illumination-related parameter μ_n with bit varying wireless channels (i.e., bit varying γ_s), VIVC denotes varying both μ_n and γ_s between successive bits. Samples from ambient carrier's complex envelope, are assumed to be drawn from a (complex) circularly symmetric normal distribution.

1) available knowledge of Φ_t and 2) estimate of Φ_t, $\widehat{\Phi}_t$, for $N_{tr} = 1, 5, 10$. It can be observed that the partially coherent, illumination agnostic rule of Eq. (45) with perfect information regarding Φ_t, offers 4 dB worst performance than the perfect CSI ML. When no information about Φ_t is available, it can be seen that for 10 training bits, the difference between the partially coherent rule utilizing perfect Φ_t and the same rule using $\widehat{\Phi}_t$ instead, is approximately 0.5 dB. When 1 training bit is used, the difference increases to ≈ 4 dB, resulting a 8 dB loss compared to perfect CSI ML.

Fig. 8 shows the performance of the detector in Eq. (52). All depicted cases assume modulated illuminator. For the special case of CIVC explained below, μ_n is assumed constant for the duration of the tag packet, while in all other cases, it changes across consecutive tag bits. It is clear that the detector for the coded case outperforms the detector used when no coding is utilized. It is also observed that in the high SNR regime, the detector offers slightly better performance, compared to perfect CSI ML detector when no coding is used. Two cases are additionally demonstrated, namely the case where both ambient signal parameter μ_n and the wireless channels vary between successive bits (resulting to varying γ_s), which will be referred to as varying illuminator varying channel (VIVC) and the case where μ_n remains constant during the packet but the channels vary among consecutive bits, resulting to varying γ_s (constant illuminator, varying channel-CIVC). In the last case, μ_n was held constant for the duration of a packet (each bit was affected by the same μ_n value) while variables $\mathsf{m}[k]$ were created as described earlier.

The performance gain offered when both parameters μ_n, γ_s vary between successive bits, is the result of the channel code being fully utilized. Constant wireless channel parameters during the transmission of multiple bits may introduce correlation between the received statistics. Thus the code may not be able to offer its best performance. In a similar manner, when the ambient carrier's parameter μ_n remains constant for the duration of the packet while the channels vary (CIVC), the same reasoning can be applied. Interestingly, Fig. 8 shows that modulation at the ambient signal assists the coded sequence detector of tag's information and radically improves performance, even though the sequence detector requires minimal information.

4) Comparison of Digital Schemes: In order to compare the two digital modulation schemes the ambient carrier is assumed to attain the form of Eq. (9). In that way, both schemes can be compared in a fair manner, given that the proposed P-FSK detection is derived based on a constant envelope modulated signal, while S-BPSK scheme can accept any modulated carrier as illuminating source (as long as Eq. (34) holds). Additionally, the same tag and wireless channel related parameters as well as bit rate ($R = 1$kbps) are assumed. The average received SNR for the S-BPSK case is defined as SNR $= \frac{\beta^2}{\tilde{\sigma}_n^2}$.

It can be seen in Fig. 6-Right that the fully coherent, P-FSK scheme outperforms S-BPSK, at the low SNR regime, for approximately 1 dB. As the SNR increases, the gap between the two schemes decreases, while for SNR $\simeq 20$ dB, the gap vanishes. This behavior may be explained by the fact that the estimation method for Φ_t in the partially coherent S-BPSK scheme is a heuristic based on the assumption of the absence of noise (Sec. IV-C). Additionally, the heuristic estimation used in S-BPSK, partially coherent detection only deals with Φ_t, while the LS estimation used in coherent detection of P-FSK, deals with the compound channel which, except Φ_t, includes tag, wireless channel and ambient carrier related parameters which are assumed constant for N_{pack},[9] bits, thus able to be estimated through short training.

B. Analog Tag Indoor and Outdoor Performance

Range performance of the tag-smartphone system was tested in indoor and outdoor scenarios. The strength of the

[9]For the coherent P-FSK scheme.

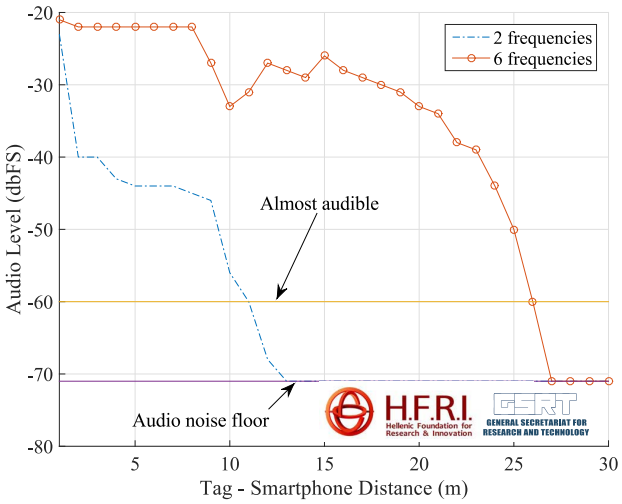

Fig. 9. Selection among up to 3 FM stations.

demodulated audio signal was reported, using the Advanced Spectrum Analyzer PRO application, running at the smartphone. This application reports audio level in a scale of dbFS, which measures the level with respect to Full Scale audio input. Anything above -20 dbFS is almost unbearable (using earphones) and anything below -70 dbFS is noise. The tests were conducted using a standard-value capacitor and a 1.5V AA battery (as power source) to ensure a constant "sensor value" (3.2 kHz) to be read.

Outdoor performance results are offered in Fig. 9. It can be seen that the tag achieves at least **26 meters** before the audio tone power drops below -60 dbFS, i.e., 10 dB above noise, resulting to demodulated backscattered signal SINR of 10 dB. At each location, the smartphone chose the frequency offering the maximum audio level at the sensor's signal among the ones offered by $L = 3$ FM illuminating stations (i.e., the smartphone tuned consecutively at $2L = 6$ frequencies and the value corresponding to the strongest sensor tone was reported). When selection was performed among two fixed frequencies/illuminating stations, performance was weaker, highlighting again the importance of selection diversity [1]; the latter comes for free for backscatter radio, given that the tag just switches and information is modulated on top of all impinged signals (from all illuminating stations) at the tag antenna. Indoor tests were also performed, demonstrating communication range of 15 meters, at impinged power of -55 dBm at the tag antenna.

VII. Conclusion

This work offered analog and digital, frequency switching techniques for ambient backscatter communication. It was shown that high performance backscatter communication is possible, even with ambient, modulated illuminators, provided that a *structured* design approach is adopted; in that way, modulation of the ambient signal can be turned to an advantage, under certain conditions. The proposed switching frequency techniques exploit existing (universal) wireless industry infrastructure and *clearly* enable ultra-low power tags/sensors, possibly powered by RF. A concrete example, based on FM, was offered. Wonderful research and entrepreneurial opportunities emerge.

Appendix
S-BPSK Decision Rule Derivation

Considering the case for $\mathrm{H}_i, i \in \{0,1\}$:

$$\max_{\tilde{\mu}_n} \ln\left[\mathrm{f}_{\mathbf{r}_{\mathrm{s},n}|\mathrm{H}_i,\tilde{\mu}_n,\Phi_\mathrm{t}}(\mathbf{r}_{\mathrm{s},n}|\mathrm{H}_i,\tilde{\mu}_n,\Phi_\mathrm{t})\right] = \max_{\tilde{\mu}_n}\left[2\ln\left(\frac{1}{\pi\tilde{\sigma}_n^2}\right) - \frac{1}{\tilde{\sigma}_n^2}||\mathbf{r}_{\mathrm{s},n} - \tilde{\mu}_n\,\mathbf{x}_i(\Phi_\mathrm{t})||_2^2\right]. \quad (61)$$

The value of the parameter $\tilde{\mu}_n$ that maximizes Eq. (61), can be given by solving the least squares problem $\tilde{\mu}_{n,\mathrm{ls}} = \arg\min_{\tilde{\mu}_n} ||\mathbf{r}_{\mathrm{s},n} - \mathbf{x}_i(\Phi_\mathrm{t})\tilde{\mu}_n||_2^2$. The solution to the aforementioned problem can be given by [34, pp. 521]:

$$\tilde{\mu}_{n,\mathrm{ls}} = \frac{\mathbf{x}_i^H(\Phi_\mathrm{t})\mathbf{r}_{\mathrm{s},n}}{||\mathbf{x}_i(\Phi_\mathrm{t})||_2^2}. \quad (62)$$

Substituting Eq. (62) to Eq. (61):

$$\begin{aligned}\max_{\tilde{\mu}_n}&\left[2\ln\left(\frac{1}{\pi\tilde{\sigma}_n^2}\right) - \frac{1}{\tilde{\sigma}_n^2}||\mathbf{r}_{\mathrm{s},n} - \tilde{\mu}_n\,\mathbf{x}_i(\Phi_\mathrm{t})||_2^2\right]\\ &= 2\ln\left(\frac{1}{\pi\tilde{\sigma}_n^2}\right) - \frac{1}{\tilde{\sigma}_n^2}||\mathbf{r}_{\mathrm{s},n} - \tilde{\mu}_{n,\mathrm{ls}}\mathbf{x}_i(\Phi_\mathrm{t})||_2^2\\ &= 2\ln\left(\frac{1}{\pi\tilde{\sigma}_n^2}\right) - \frac{1}{\tilde{\sigma}_n^2}\left(||\mathbf{r}_{\mathrm{s},n}||_2^2 - \frac{|\mathbf{r}_{\mathrm{s},n}^H\mathbf{x}_i(\Phi_\mathrm{t})|^2}{||\mathbf{x}_i(\Phi_\mathrm{t})||_2^2}\right). \quad (63)\end{aligned}$$

Using Eq. (63) and exploiting the fact that $||\mathbf{x}_i(\Phi_\mathrm{t})||_2^2 = 2$, the following is obtained:

$$\begin{aligned}&\max_{\tilde{\mu}_n}\left[2\ln\left(\frac{1}{\pi\tilde{\sigma}_n^2}\right) - \frac{1}{\tilde{\sigma}_n^2}||\mathbf{r}_{\mathrm{s},n} - \tilde{\mu}_n\,\mathbf{x}_i(\Phi_\mathrm{t})||_2^2\right]\\ &= 2\ln\left(\frac{1}{\pi\tilde{\sigma}_n^2}\right) - \frac{1}{\tilde{\sigma}_n^2}\left(||\mathbf{r}_{\mathrm{s},n}||_2^2 - \frac{1}{2}|\mathbf{r}_n^H\mathbf{x}_i(\Phi_\mathrm{t})|^2\right)\\ &= 2\ln\left(\frac{1}{\pi\tilde{\sigma}_n^2}\right) - \frac{1}{\tilde{\sigma}_n^2}||\mathbf{r}_{\mathrm{s},n}||_2^2\\ &\quad + \frac{1}{2\tilde{\sigma}_n^2}\left|\left(r_{\mathrm{s},n}^+\right)^*\mathrm{e}^{\mathrm{j}(\Phi_\mathrm{t}+\Phi_i)} + \left(r_{\mathrm{s},n}^-\right)^*\mathrm{e}^{-\mathrm{j}(\Phi_\mathrm{t}+\Phi_i)}\right|^2\\ &= 2\ln\left(\frac{1}{\pi\tilde{\sigma}_n^2}\right) - \frac{1}{\tilde{\sigma}_n^2}||\mathbf{r}_{\mathrm{s},n}||_2^2\\ &\quad + \frac{1}{2\tilde{\sigma}_n^2}\left(|r_{\mathrm{s},n}^+|^2 + 2\Re\left\{\left(r_{\mathrm{s},n}^+\right)^*\left(r_{\mathrm{s},n}^-\right)\mathrm{e}^{\mathrm{j}2(\Phi_\mathrm{t}+\Phi_i)}\right\} + |r_{\mathrm{s},n}^-|^2\right)\\ &= 2\ln\left(\frac{1}{\pi\tilde{\sigma}_n^2}\right) - \frac{1}{\tilde{\sigma}_n^2}||\mathbf{r}_{\mathrm{s},n}||_2^2\\ &\quad + \frac{1}{2\tilde{\sigma}_n^2}\left(||\mathbf{r}_{\mathrm{s},n}||_2^2 + 2\Re\left\{\left(r_{\mathrm{s},n}^+\right)^*\left(r_{\mathrm{s},n}^-\right)\mathrm{e}^{\mathrm{j}2(\Phi_\mathrm{t}+\Phi_i)}\right\}\right)\\ &= 2\ln\left(\frac{1}{\pi\tilde{\sigma}_n^2}\right) - \frac{1}{2\tilde{\sigma}_n^2}||\mathbf{r}_{\mathrm{s},n}||_2^2\\ &\quad + \frac{1}{\tilde{\sigma}_n^2}\Re\left\{\left(r_{\mathrm{s},n}^+\right)^*\left(r_{\mathrm{s},n}^-\right)\mathrm{e}^{\mathrm{j}2(\Phi_\mathrm{t}+\Phi_i)}\right\}. \quad (64)\end{aligned}$$

REFERENCES

[1] G. Vougioukas and A. Bletsas, "24μW26m range batteryless backscatter sensors with FM remodulation and selection diversity," in *Proc. IEEE RFID Techn. Appl. (RFID-TA)*, Warsaw, Polland, Sep. 2017, pp. 237–242.

[2] G. Vougioukas, P. N. Alevizos, and A. Bletsas, "Coherent detector for pseudo-FSK backscatter under ambient constant envelope illumination," in *Proc. IEEE Workshop Signal Process. Adv. Wireless Commun. (SPAWC)*, Kalamata, Greece, Jun. 2018, pp. 1–5.

[3] H. Stockman, "Communication by means of reflected power," *Proc. IRE*, vol. 36, no. 10, pp. 1196–1204, Oct. 1948.

[4] G. Vannucci, A. Bletsas, and D. Leigh, "A software-defined radio system for backscatter sensor networks," *IEEE Trans. Wireless Commun.*, vol. 7, no. 6, pp. 2170–2179, Jun. 2008.

[5] E. Kampianakis, J. Kimionis, K. Tountas, C. Konstantopoulos, E. Koutroulis, and A. Bletsas, "Wireless environmental sensor networking with analog scatter radio and timer principles," *IEEE Sensors J.*, vol. 14, no. 10, pp. 3365–3376, Oct. 2014.

[6] C. Konstantopoulos, E. Koutroulis, N. Mitianoudis, and A. Bletsas, "Converting a plant to a battery and wireless sensor with scatter radio and ultra-low cost," *IEEE Trans. Instrum. Meas.*, vol. 65, no. 2, pp. 388–398, Feb. 2016.

[7] S.-N. Daskalakis, S. D. Assimonis, E. Kampianakis, and A. Bletsas, "Soil moisture scatter radio networking with low power," *IEEE Trans. Microw. Theory Tech.*, vol. 64, no. 7, pp. 2338–2346, Jul. 2016.

[8] P. N. Alevizos, A. Bletsas, and G. N. Karystinos, "Noncoherent short packet detection and decoding for scatter radio sensor networking," *IEEE Trans. Commun.*, vol. 65, no. 5, pp. 2128–2140, May 2017.

[9] J. Kimionis, A. Bletsas, and J. N. Sahalos, "Design and implementation of RFID systems with software defined radio," in *Proc. 6th Eur. Conf. Antennas Propag. (EUCAP)*, Mar. 2012, pp. 3464–3468.

[10] J. Kimionis, A. Bletsas, and J. N. Sahalos, "Increased range bistatic scatter radio," *IEEE Trans. Commun.*, vol. 62, no. 3, pp. 1091–1104, Mar. 2014.

[11] N. Fasarakis-Hilliard, P. N. Alevizos, and A. Bletsas, "Coherent detection and channel coding for bistatic scatter radio sensor networking," *IEEE Trans. Commun.*, vol. 63, no. 5, pp. 1798–1810, May 2015.

[12] P. N. Alevizos, K. Tountas, and A. Bletsas, "Multistatic scatter radio sensor networks for extended coverage," *IEEE Trans. Wireless Commun.*, vol. 17, no. 7, pp. 4522–4535, Jul. 2018.

[13] V. Liu, A. Parks, V. Talla, S. Gollakota, D. Wetherall, and J. R. Smith, "Ambient backscatter: Wireless communication out of thin air," in *Proc. ACM SIGCOMM*, Hong Kong, 2013, pp. 39–50.

[14] A. N. Parks, A. Liu, S. Gollakota, and J. R. Smith, "Turbocharging ambient backscatter communication," in *Proc. ACM SIGCOMM*, Chicago, IL, USA, 2014, pp. 619–630.

[15] A. Wang, V. Iyer, V. Talla, J. R. Smith, and S. Gollakota, "FM backscatter: Enabling connected cities and smart fabrics," in *Proc. USENIX Symp. Netw. Syst. Design Implement.*, Boston, MA, USA, Mar. 2017, pp. 243–258.

[16] M. A. Varner, R. Bhattacharjea, and G. D. Durgin, "Perfect pulses for ambient backscatter communication," in *Proc. IEEE RFID*, Phoenix, AZ, USA, May 2017, pp. 13–19.

[17] G. Wang, F. Gao, R. Fan, and C. Tellambura, "Ambient backscatter communication systems: Detection and performance analysis," *IEEE Trans. Commun.*, vol. 64, no. 11, pp. 4836–4846, Nov. 2016.

[18] J. Qian, F. Gao, G. Wang, S. Jin, and H. Zhu, "Noncoherent detections for ambient backscatter system," *IEEE Trans. Wireless Commun.*, vol. 16, no. 3, pp. 1412–1422, Mar. 2017.

[19] J. Qian, F. Gao, G. Wang, S. Jin, and H. Zhu, "Semi-coherent detection and performance analysis for ambient backscatter system," *IEEE Trans. Commun.*, vol. 65, no. 12, pp. 5266–5279, Dec. 2017.

[20] G. Yang, Y.-C. Liang, R. Zhang, and Y. Pei. (2017). "Modulation in the air: Backscatter communication over ambient OFDM carrier." [Online]. Available: http://arxiv.org/abs/1704.02245

[21] D. Darsena, G. Gelli, and F. Verde, "Modeling and performance analysis of wireless networks with ambient backscatter devices," *IEEE Trans. Commun.*, vol. 65, no. 4, pp. 1797–1814, Jan. 2017.

[22] N. Van Huynh, D. T. Hoang, X. Lu, D. Niyato, P. Wang, and D. I. Kim. (Dec. 2017). "Ambient backscatter communications: A contemporary survey." [Online]. Available: https://arxiv.org/abs/1712.04804

[23] X. Lu, P. Wang, D. Niyato, D. I. Kim, and Z. Han, "Wireless networks with RF energy harvesting: A contemporary survey," *IEEE Commun. Surveys Tuts.*, vol. 17, no. 2, pp. 757–789, 2nd Quart., 2015.

[24] S. Bi, C. K. Ho, and R. Zhang, "Wireless powered communication: Opportunities and challenges," *IEEE Commun. Mag.*, vol. 53, no. 4, pp. 117–125, Apr. 2015.

[25] H. Taub and D. L. Schilling, *Principles of Communication Systems*, 2nd ed. New York, NY, USA: McGraw-Hill, 1986.

[26] J. G. Proakis and M. Salehi, *Communication Systems Engineering*, 2nd ed. Upper Saddle River, NJ, USA: Prentice-Hall, 2001.

[27] D. J. Sakrison, *Communication Theory: Transmission of Waveforms and Digital Information*. New York, NY, USA: Wiley, 1968.

[28] Microchip Technology Inc. *PIC16LF145X Series Datasheet*. Accessed: Oct. 3, 2018. [Online]. Available: http://ww1.microchip.com/downloads/en/DeviceDoc/40001639B.pdf

[29] SiTime Corporation. *SiT1576 μPower Oscillator Datasheet*. Accessed: Oct. 3, 2018. [Online]. Available: https://www.sitime.com/datasheet/SiT1576

[30] R. J. M. Vullers, R. van Schaijk, I. Doms, C. van Hoof, and R. Mertens, "Micropower energy harvesting," *Solid-State Electron.*, vol. 53, no. 7, pp. 684–693, 2009.

[31] G. Vougioukas, A. Dimitriou, A. Bletsas, and J. Sahalos, "Practical energy harvesting for batteryless ambient backscatter sensors," *Electronics*, vol. 7, no. 6, p. 95, Jun. 2018.

[32] D. Tse and P. Viswanath, *Fundamentals of Wireless Communication*. New York, NY, USA: Cambridge Univ. Press, 2005.

[33] F. W. J. Olver, D. W. Lozier, R. F. Boisvert, and C. W. Clark, *NIST handbook of mathematical functions*. New York, NY, USA: Cambridge Univ. Press, 2010.

[34] S. M. Kay, *Fundamentals of Statistical Signal Processing: Estimation Theory*, vol. 1. Upper Saddle River, NJ, USA: Prentice-Hall, 1993.

[35] S. Kay, *Fundamentals of Statistical Signal Processing: Detection theory*. Upper Saddle River, NJ, USA: Prentice-Hall, 1998.

[36] G. Vougioukas and A. Bletsas, *Smartphone Reception of μWatt, m-km Range Backscatter Resistive/Capacitive Sensors with Ambient FM Remodulation & Selection Diversity* (Elements Series), N. B. Carvalho, Ed. Cambridge, U.K.: Cambridge Univ. Press, Mar. 2018.

[37] MathWorks Inc. *SNR Function Documentation*. (Feb. 13, 2018). [Online]. Available: https://www.mathworks.com/help/signal/ref/snr.html

[38] A. S. Willsky, G. W. Wornell, and J. H. Shapiro, "Stochastic processes, detection, and estimation," Course Notes, MIT Opencourseware, 2003.

Georgios Vougioukas received the 5-year Diploma degree in electrical and computer engineering from the Technical University of Crete, Greece, in 2016, where he is currently pursuing the Ph.D. degree. His research interests include methods for ultra-low power wireless communication, signal processing for backscatter communication, energy harvesting, sensing, analog & digital system design and implementation. He was a co-recipient of the 2017 IEEE International Conference on RFID Technology & Applications (RFID-TA) Best Student Paper Award. He has been distinguished as an Exemplary Reviewer of 2017 by the Editorial Board of the IEEE TRANSACTIONS ON WIRELESS COMMUNICATIONS.

Aggelos Bletsas received the Diploma degree (Hons.) in electrical and computer engineering from the Aristotle University of Thessaloniki, Greece, in 1998, and the S.M. and Ph.D. degrees from the Massachusetts Institute of Technology, Cambridge, MA, USA, in 2001 and 2005, respectively. He is currently an Associate Professor with the School of Electrical & Computer Engineering, Technical University of Crete, Greece. His research interests span the broad area of scalable wireless communications and sensors networking. He was a co-recipient of the IEEE Communications Society 2008 Marconi Prize Paper Award in Wireless Communications, and also a recipient of various Best Student Paper Awards, e.g., in the IEEE RFID-TA 2011, the ICASSP 2015, the RFID-TA 2017, and the MOCAST 2018.